

**AES/TGP/13-27** Seismic Attribute Analysis of the Upper Cretaceous below the Tambaredjo oil field, Suriname

**August 22<sup>nd</sup> Rishitesh Roepnarain**

Title : Seismic Attribute Analysis of the Upper Cretaceous  
below the Tambaredjo oil field, Suriname

Author(s) : Rishitesh Roepnarain

Date : August 2013  
Professor(s) : Stefan Luthi  
Supervisor(s) : August Nelson  
TA Report number : AES/TGP/13-27

Postal Address : Section for Applied Earth Science  
Department of Geoscience & Engineering  
Delft University of Technology  
P.O. Box 5028  
The Netherlands

Telephone : (31) 15 2781328 (secretary)  
Telefax : (31) 15 2781189

Copyright ©2013 Section for **Applied Earth Science**

*All rights reserved.  
No parts of this publication may be reproduced,  
Stored in a retrieval system, or transmitted,  
In any form or by any means, electronic,  
Mechanical, photocopying, recording, or otherwise,  
Without the prior written permission of the  
Section for **Applied Earth Science***

**Seismic Attribute Analysis of the Upper Cretaceous below the  
Tambaredjo oil field, Suriname**

**By**

**Rishitesh Roepnarain**

**A thesis submitted in partial fulfilment of the requirements for the degree of**

**Master of Sciences in Applied Geophysics  
Joint Master's Idea League**

**at the**

**Delft University of Technology**

**Delft, The Netherlands**

**2013**

The thesis of Rishitesh Roepnarain is approved by the Thesis Examining Committee

---

**Stefan Luthi** (Chairman & Supervisor)

---

**August Nelson** (External Supervisor)

---

**Gerhard Diephuis** (Advisor)

---

**Stewart Greenhalgh** (Advisor)

**Delft University of Technology**

**2013**

# Table of Content

Preface

Summary

List of Figures and Tables

Abbreviations

1	Introduction .....	1
1.1	Seismic data .....	4
2	Geologic framework .....	6
2.1	Regional geology .....	6
2.2	Sequence stratigraphy of the Cretaceous Nickerie Formation .....	8
2.2.1	Lower Nickerie Formation .....	10
2.2.2	Upper Nickerie Formation .....	10
1.1.1	2.2.3 Upper Cretaceous unconformity (Cretaceous-Tertiary Boundary) .....	11
2.3	Faults below the Tambaredjo oil field .....	12
3	Seismic Attributes .....	14
3.1	Introduction .....	14
3.2	Classification of attributes .....	14
3.3	Attribute Analysis in Clastic Depositional Systems .....	16
3.4	Evaluation of Attributes .....	19
3.4.1	Instantaneous Amplitude .....	20
3.4.2	Cosine of Instantaneous Phase .....	20
3.4.3	Instantaneous frequency .....	21
3.4.4	Instantaneous Q factor (quality factor) .....	22
3.4.5	Variance .....	23
3.4.6	RMS Energy .....	23

3.4.7	Coherence and Similarity .....	23
3.4.8	Thin Bed Indicator .....	24
3.4.9	Spectral Decomposition .....	25
4	Methodology.....	26
4.1	Steering cube .....	26
4.2	Horizon Interpretation .....	27
4.3	Horizon cube.....	28
4.4	Seismic Attribute Analysis .....	29
4.5.	Combination of seismic attributes .....	29
5	Results and Discussion .....	31
6	Conclusion and Recommendations.....	44
6.1	Conclusion.....	44
6.2	Recommendations .....	45
	References .....	46
	Appendices .....	49
Appendix A	Seismic wavelet, polarity and resolution .....	50
Appendix B	Seismic Attribute Maps.....	54

## **Preface**

In order to finalize the IDEA League Joint Master in Applied Geophysics, I had to conduct a graduation research. The research was carried out with three-dimensional seismic data provided by the national oil company of Suriname, Staatsolie Maatschappij Suriname N.V. I had the opportunity to use this data set in order to extract seismic attributes for the study of the Cretaceous interval below the Tambaredjo oil field. This report contains the results of this research and is divided into six chapters. The first chapter describes the purpose and objective of this study. In the second chapter the geology and stratigraphy of the study area are described. Chapter 3 gives an evaluation of the attributes used in this study. In the fourth chapter the methodology and workflow of this analysis are described. After this the results obtained are discussed in chapter 5. This report is completed with a conclusion and some recommendations.

This research would not have been possible if I did not get the opportunity from Staatsolie Maatschappij Suriname N.V. to use their data. Furthermore they gave me a chance to do a two month internship there. Especially Mr. August Nelson, the head of the Exploration Division, and his staff, gave me a welcoming heart and a lot of support during my thesis.

I am also very thankful to my supervisor, professor Stefan Luthi. His insights and support enlightened my project.

My special thanks go to dGB Earth Sciences, for the use of their software OpendTect. Further they helped me with all the software problems I got during my thesis. One person who I owe a lot to is Eric Bouanga. Without his constant support and dedication, I would not have finished this project.

Finally I would like to thank my family and friends who were of great support during the writing of my thesis. Without them my life would be so incomplete.

## Summary

The Tambaredjo field is the largest oil field in Suriname. Since 1982 the state oil company, Staatsolie Maatschappij Suriname N.V., has been extracting oil from the Palaeocene reservoir sands. More recently there has been a growing interest in the Cretaceous interval below the reservoir sands. However, not much data is available from this interval. With this study an attempt is made to utilize seismic attributes from a 3-D seismic survey for identifying geological features of interest and predicting lithofacies and their distribution within the Upper Cretaceous below a part of the Tambaredjo oilfield. The approach of this attribute analysis was deterministic. Before extraction of the attributes a literature study was conducted in order to find and select appropriate seismic attributes. These attributes were then calculated in an interval marked by two seismic horizons, the Top of the Cretaceous and second horizon lying 60 ms (two-way-travel time) below the Top of the Cretaceous. Within this interval, flattened (expected) chronostratigraphic slices were created using a Horizon Cube and the Wheeler transform. The calculated attributes were then displayed and analysed along these flattened slices. The analysis of the attributes resulted in the identification of interesting geological features such as channels, which may contain potential reservoir sands. Furthermore using a selection of attributes, a segmentation analysis based on neural networks has been applied. This resulted in clustered areas of comparable seismic responses, which could indicate the distribution of different lithofacies or lithologies.

## List of Figures and tables

**Figure 1.1:** Map of the coastal area of Suriname, showing the Tambaredjo and Calcutta fields (Courtesy Staatsolie Maatschappij Suriname N.V.).

**Figure 1.2:** Overview of the 3D survey area (shown in the rectangle). The blue line in the south of this field represents the Saramacca river (modified from Schram De Jong, 2003).

**Table 1.1:** Main parameters of the 3D seismic survey.

**Figure 1.3:** Image of the inline 340. This image shows the poor resolution of the Cretaceous interval compared to the shallower Tertiary section. Further a section (blurry section in rectangle) is shown where the seismic data is bad thorough the whole time interval. The top of the Cretaceous is marked by the blue arrow.

**Figure 2.1:** The Suriname-Guyana Basin indicated by the dotted line (from: [www.staatsolie.com](http://www.staatsolie.com))

**Figure 2.2:** N-S Cross-section from the Guyana Shield to the Atlantic Ocean showing the Corantijn Group and the location of the Tambaredjo field. (modified, courtesy of Staatsolie Maatschappij Suriname N.V.).

Figure 2.3: Stratigraphic column onshore Suriname with different stratigraphic markers and reservoir units within the Tambaredjo oil field (Courtesy of Staatsolie Maatschappij Suriname N.V.)

**Figure 2.4:** Faults identified in the 3D seismic area. The different colours represent different fault patterns identified. Blue lines → EW trending faults, Red lines → NE-SW trending faults, brown lines → ENE-WSW trending faults and green → NS trending faults. Imaged modified from Kisoensingh (2009).

**Figure 3.1:** Sketch of an actual seismic trace and it Hilbert transform, quadrature seismic trace (Taner, 1992)

**Figure 4.1:** Part of crossline 20 showing the Horizon cube (blue lines) with its bounding surfaces (pink and white line) and the 14 intermediate horizons created by a data driven method. The actual top of Cretaceous is also pointed out in this image

**Figure 5.1:** Instantaneous amplitude stratal slice of the Top Cretaceous. The black rectangle delineates an ESE-NNW trending channel feature, whereas the green rectangle encloses a linear NE-SW structure. Please note that the width and length of the slice correspond to the dimensions of the survey area. The width is 8 kilometers and the length 10.4 kilometers. These dimensions are valid for all the slices shown in this chapter.

**Figure 5.2:** Similarity stratal slice (left) and fault map of the Tambaredjo 3D area (right) (modified from Kisoensingh, 2009). On the left image, red box delineates the channel feature; black square delineates the linear structure. Further arrows indicate different faults. Blue arrow → EW trending fault system, red arrow → NE-SW trending fault and brown arrow → broederschapsbreuk.

**Figure 5.3:** Cosine of instantaneous phase of the Top of Cretaceous. Top arrow indicates the EW trending fault system and bottom two arrows show the 'Broederschapsbreuk'. White line indicates cross section through the linear structure.

**Figure 5.4:** Image of the inline number 1203. This inline cuts through the linear structure seen in figure 5.3. The pink line represents the Top of Cretaceous and the white line the 60 ms shifted horizon.

**Figure 5.5:** Image of inline number 1203. This line cuts through the linear structure seen in figure 5.3. The blue circles, enclose a possible channel feature. The area in the middle pointed out with blue arrows coincides with areas of high amplitudes.

**Figure 5.6:** RMS energy slice of the Top of Cretaceous. The purple arrow indicates high RMS energy, related to high amplitudes, in the middle of the linear structure (within the white box).

**Figure 5.7:** Instantaneous frequency slice of the Top of Cretaceous. Northern channel feature has been edited to visually enhance the image. The edges of the channel have been coloured purple. The middle of the linear structure (purple box) is indicated by a purple arrow.

**Figure 5.8:** Thin bed indicator slice of the Top of Cretaceous. Orange box delineates the southern channel feature with anomalies in thin bed indicator.

**Figure 5.9:** RGB blend of RMS energy (red colour), instantaneous phase (green) and instantaneous frequency (blue).

**Figure 5.10:** Similarity stratal slice below the Top of Cretaceous. Faults are indicated by blue arrows. In the black rectangular two channels can be seen. The edges of these channels are highlighted by red and orange colours.

**Figure 5.11:** Cosine of the instantaneous phase stratal slice below the Top of the Cretaceous. White rectangle shows the area where the linear structure was found at the Top of the Cretaceous. Black rectangle delineates area where high amplitudes can be found in figure 5.12..

**Figure 5.12:** RMS energy stratal slice below the Top of the Cretaceous. Black rectangle highlights the area where most likely the channel features occur, showing high amplitudes. The white rectangle highlights section of high amplitudes in the southeastern part of the study area. The black arrows indicate faults.

**Figure 5.13:** Instantaneous frequency stratal slice below the Top of the Cretaceous. Red rectangle marks area with high amplitudes. Black rectangles marks frequency anomalies at NNW – SSE fault location.

**Figure 5.14:** Cosine of instantaneous phase. This is the pattern from the second stratal slice below the Top of Cretaceous and onwards.

**Figure 5.15:** UVQ using the instantaneous frequency, RMS energy and cosine of instantaneous attribute. The UVQ is run along the Top of the Cretaceous. Black rectangle depicts possibly channel feature containing sand. Green rectangle shows a possible belt.

**Figure: A.1:** Terminology used for seismic wavelets (Haverkamp, 2002)

**Figure A.2:** The minimum phase and zero phase wavelets. In this image it is clearly shown that the interface with acoustic impedance contrast coincides with the maximum amplitude of a zero phase wavelet and the start position of a minimum phase wavelet (Veeken, 2007).

**Figure A.3:** Density display of zero-phase wavelet in SEG positive polarity (modified from lecture notes Diephuis, 2012)

**Figure A.4:** Density display of zero-phase wavelet in SEG negative polarity (modified from lecture notes Diephuis, 2012)

**Figure A.5:** Example of constructive and destructive interference for a minimum-phase wavelet (Haverkamp, 2002)

## Abbreviations

<b>Short form</b>	<b>For</b>
3D	Three dimensional space
Km <sup>2</sup>	Square kilometre(s)
Km	Kilometre(s)
s	Seconds
ms	Milliseconds
m	Metre(s)
N	North
W	West
S	South
E	East
STOIP	Stock Tank Oil Initially In Place

# 1 Introduction

The Tambaredjo field (Figure 1.1) is an oilfield located about 30 km west of Paramaribo. The first discovery of oil in the Tambaredjo field was in 1961, but due to low production rates and crude oil gravity, development of the field didn't start until 1981. Production started in 1982 with 116 barrels of oil per day and currently Staatsolie Maatschappij Suriname N.V. produces nearly 16000 barrels of oil per day mainly from the Tambaredjo field (900 mbs STOIP) and also from a smaller Calcutta field (150 mbs STOIP). The main reservoir units are Palaeocene T-sands for the Tambaredjo field and Eocene and Miocene sands for the Calcutta field (POC Team, 2008).



**Figure 2.1:** Map of the coastal area of Suriname, showing the Tambaredjo and Calcutta fields (Courtesy Staatsolie Maatschappij Suriname N.V.).

Recently, exploration wells in the Tambaredjo field have shown oil traces in the Cretaceous interval. These oil occurrences in the Cretaceous were also visible in other exploration wells in other parts of Suriname, such as Weg Naar Zee, Coesewijne and Commewijne. After conducting a geochemical analysis on extracted oil samples from the Cretaceous interval, it was shown that the Cretaceous oil is charged from a different source rock than the Canje

Cenomanian-Turonian source rock charging the known reservoirs of the Tambaredjo and Calcutta fields. This finding encouraged the belief that the Cretaceous play was part of a much older petroleum system than the proven Cenomanian Turonian petroleum system (POC Team, 2008). The focus of exploration programmes within Staatsolie Maatschappij Suriname N.V. thus shifted a bit towards the Cretaceous interval. But until recently, not much research has been conducted on this Lower Cenozoic interval. This was most likely as a result of its perceived low hydrocarbon potential and lack of well information. Important aspects to study would be the distribution of lithofacies. Also the identification of certain geological features, such as sand bodies, could help the prospectivity of hydrocarbons in the Cretaceous and increase the chances of drilling successes.

Since their introduction in the 1970's, seismic attributes have been helpful in seismic data interpretation (Taner, 1992). From that time on numerous seismic attributes have been developed and made accessible to geoscientists for purposes such as lithofacies prediction and reservoir property prediction. Seismic attributes are calculated from seismic data. In 2001 a high resolution three-dimensional (3D) seismic data set of the Tambaredjo field became available. With this data set it could thus be possible to conduct a seismic attribute analysis to extract more information from the Cretaceous.

Pigott et al. (2013) have identified two approaches for doing an attribute analysis. They call it the stochastic and deterministic approach. The stochastic approach is where as many attributes as available are calculated on the area of interest. It is then checked which of the attributes relate the best to the various geological hypotheses produced. This approach can provide a quick solution without much a priori knowledge, but it is also subject to misinterpreting the many geological possibilities produced. The deterministic approach, however, demands a thorough geological and geophysical understanding, before selecting appropriate attributes, which are then calculated over the area of interest.

An attribute analysis can have two purposes. It can either be half-quantitative and/ or it can be qualitative. In a half quantitative attribute analysis an attempt is made to predict the distribution of physical properties(e.g. porosity, permeability, thickness) of the layer in interest, whereas in a qualitative analysis the purpose is to find geobodies or geological features such as channels, point bars etc. (Xia et al., 2013).

From the paragraphs above, the aim of this study can be formulated. The purpose of this study is to conduct a deterministic and qualitative attribute analysis in order to delineate geological

features of interest as well as finding lithofacies and their distribution within the upper Cretaceous interval of the Tambaredjo oil field. Expected also, is to gain a better understanding of the geology of the Upper Cretaceous. A part of this study will also concentrate on selecting appropriate attributes for this analysis. The selection of attributes will be based on a literature review, geological review and evaluation of attributes.

The area of investigation includes the upper 20 meters of the Cretaceous and is located where the 3D seismic survey was conducted. This area is part of the Tambaredjo field and in figure 1.2 it is outlined by a rectangle. The area length and width are respectively 10.4 and 8 kilometres. Because of a short amount of time, not the whole Upper Cretaceous interval could be evaluated. Therefore only the upper 20 meters of the Cretaceous interval were chosen.

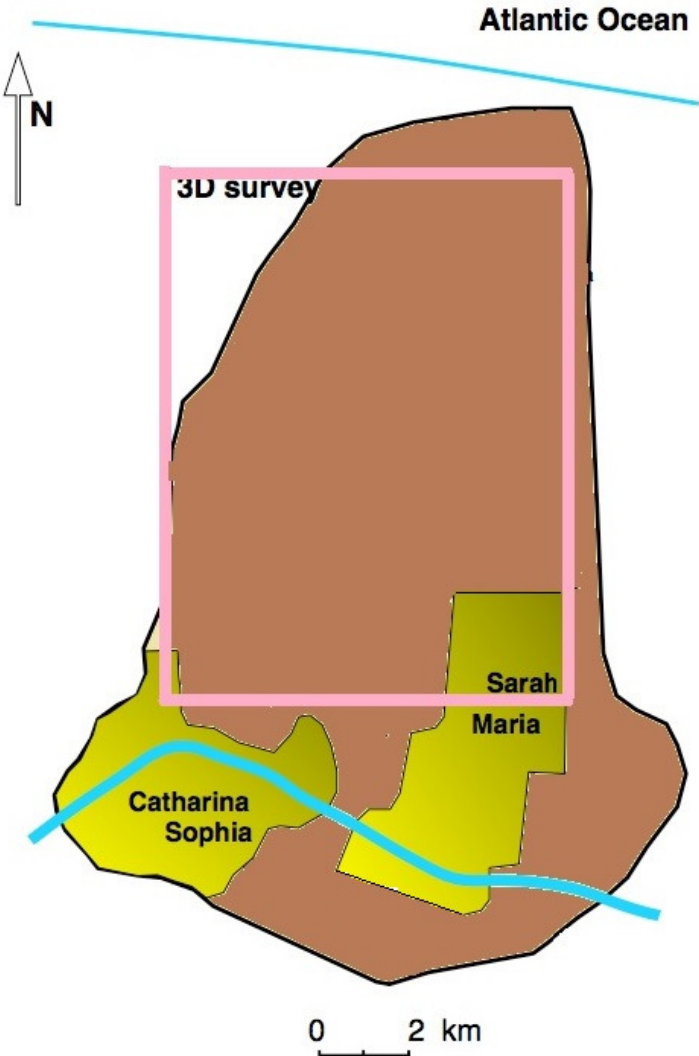


**Figure 1.2:** Overview of the 3D survey area (shown in the rectangle). The blue line in the south of this field represents the Saramacca river (modified from Schram De Jong, 2003).

## 1.1 Seismic data

The 3D high resolution seismic data was acquired in 2001. This acquisition was done with the objective to get a detailed image of the subsurface for improved oil recovery from the existing reservoir sands. In 2012 this data was reprocessed for resolution improvement, which was focused on the shallower Tertiary section.

Noticeable, is the poorer seismic data quality in the Cretaceous interval compared to the shallower parts of the section (Figure 1.3). This could be due to the fact that the focus of acquisition and processing of the seismic data had been imaging of the Tertiary reservoir sands. Another reason for this bad quality could be the absorption of high frequencies with depth. The Regional Exploration Team (RET) at Staatsolie Maatschappij Suriname N.V. has found frequencies up to 120 Hz in the shallower Tertiary interval, whereas the Cretaceous interval contain frequencies up to 70 Hz (RET, 2012).

Another observation is that at some locations it can be seen that the data is blurry throughout the whole section. These irregular disturbances start from the surface and affect the whole sedimentary section beneath. According to Kisoensingh (2009), who worked with the old 3D data set, it is likely that this is a result of processing artifacts, since surface objects could have not induced it (the whole area consists mostly of grass swamp areas).

During reprocessing a pre-stack time migration was also conducted. This pre-stack time migrated data is used for this seismic attribute analysis. In Table 1.1, the main parameters of the seismic survey can be seen.

<b>Survey dimensions</b>	10.4 by 8 km
<b>Area</b>	83.2 km <sup>2</sup>
<b>Type of receivers used</b>	Hydrophones
<b>Time window</b>	1000 ms
<b>Inline range</b>	3-1666
<b>Crossline range</b>	5-1284
<b>Inline spacing</b>	6.25 m

<b>Crossline spacing</b>	6.25 m
<b>Number of traces</b>	2128640
<b>Type of wavelet</b>	Zero phase
<b>Polarity</b>	SEG
<b>Estimated vertical resolution</b>	2.5 – 4 m

**Table 1.1:** Main parameters of the 3D seismic survey.

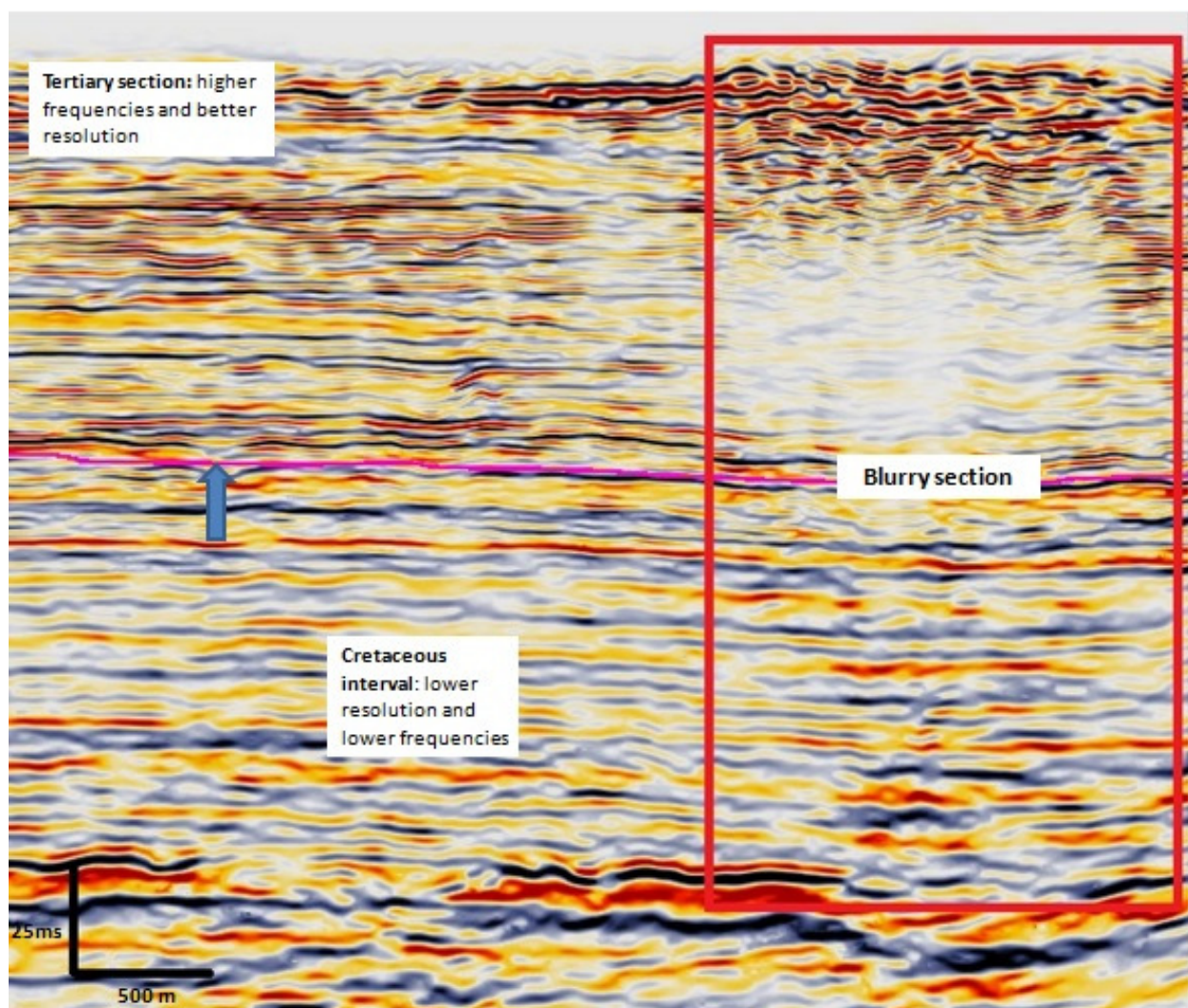


**Figure 1.3:** Image of the inline 340. This image shows the poor resolution of the Cretaceous interval compared to the shallower Tertiary section. Further a section (blurry section in rectangle) is shown where the seismic data is bad throughout the whole time interval. The top of the Cretaceous is marked by the blue arrow.

# 2 Geologic framework

## 2.1 Regional geology

The sediments of the Tambaredjo field are part of the Guyana Basin. This basin is a passive margin basin on the northeast coast of South America. It consists of offshore and coastal areas of French Guyana, Suriname, Guyana and the eastern part of Venezuela. The part of the basin encompassing the territorial waters of Suriname is named as the Suriname-Guyana basin (Figure 2.1). The basin evolved in three main tectonic phases from the Early Jurassic-Early Cretaceous with the opening of the Atlantic Ocean. In the east and west, the basin is bordered respectively by the Demerara rise and the Antillean Arch. In the south the sediments of the basin onlap the Guiana Shield, a crystalline Proterozoic basement. Offshore the sediment package becomes thicker as the basement grows deeper (Van Strien(2010), Workman & Birnie (2007), Halliburton (2009)).

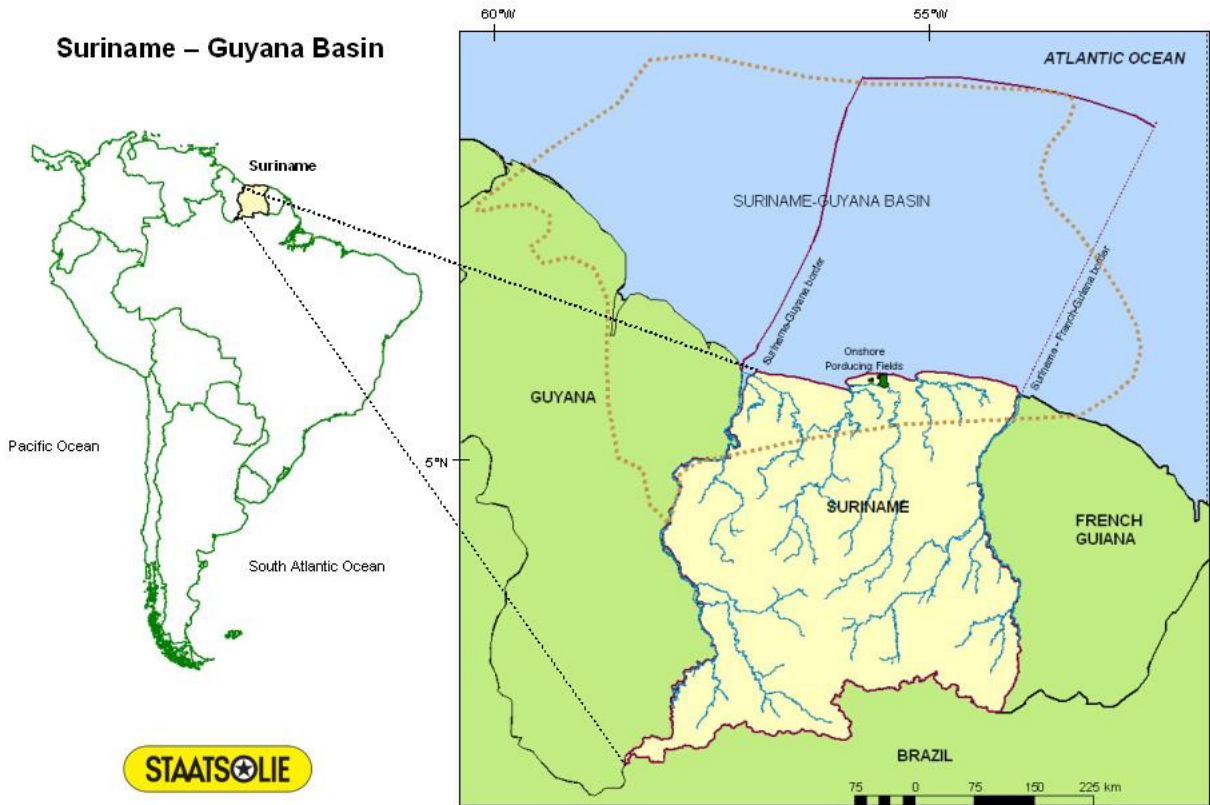


Figure 2.1: The Suriname-Guyana Basin indicated by the dotted line (from: www.staatsolie.com)

The structural development and depositional history of the Guiana basin are a result of three tectonic phases from Early Jurassic to Late Cretaceous. The oldest of them is the Central Atlantic Phase. This phase started in the Early Jurassic and is governed by a NE-SW trending rift system in the Central Atlantic. This rift system was initiated by the North Atlantic rift system, which started the separation between North America and Laurasia and eventually extended southwards. The southern extent of the NE-SW rifting system is the Takutu Graben, lying at the border between Guyana and Brazil. In the Middle Jurassic the drifting stage proceeded after rifting and this resulted in the creation of the North and Central Atlantic. An important structure in Suriname developed from the rifting and drifting is the Bakhuis horst in NW Suriname. This horst structure plays an important role for the entrapment of oil in the Tambaredjo field (Kisoensingh, 2009; Van Strien, 2010).

The second tectonic phase, the Early Cretaceous Phase, started in the beginning of the Cretaceous (Aptian-Albian) and initiated rifting between the South American Plate and African plate. This rifting phase propagated from the south northwards and due to relative plate motions caused a counter-clockwise movement of the African plate. This movement resulted in the development of compressional structures in the region. Compressional structures on the Demerara plateau, a submarine plateau off the coast of French Guiana and Suriname, are a remnant of this Early Cretaceous inversion. Another effect of this compressional event was the Aptian-Albian unconformity in the regional stratigraphy throughout the basin. Onshore this unconformity forms the boundary of the lower Cretaceous sediments (Van Strien, 2010; Kisoensingh, 2009).

After this compressional phase, the Equatorial Atlantic Phase proceeded. This phase proceeded from the Albian onwards and resulted in the drifting away of the African plate from the South American plate. During this phase an extensional regime prevailed along the Surinamese coast. Van Strien (2010) states that Albian strata are not found onshore Suriname. Albian strata are found in the Guiana basin, but pinches out approximately 30 km off the coast. During the Equatorial Atlantic Phase abundant sediments, such as marine clastics and carbonates, were deposited in the Guiana basin. Also the world-class Cenomanian source rocks were deposited during this phase (POC Team, 2008; Kisoensingh, 2009; Van Strien, 2010).

A later tectonic event influencing the deposition in the Guiana basin is the subduction of the Pacific plate below the South American plate during Mid-Miocene. The subduction gave rise to the uplift of the Andes mountain chain in the western part of South America. The uplift

changed the drainage pattern of the Amazon from westward to an eastern drainage system (Potter, 1997). This switch in drainage system resulted in a more clay-rich supply of sediments to the Guiana basin. Along the coast of Suriname, this clay-rich supply is characterized by the westward migrating mudbanks (POC Team, 2008).

### 2.2 Sequence stratigraphy of the Cretaceous Nickerie Formation

In the onshore area of Suriname the sediments of the Guiana basin are part of the Corantijn Group. The group consists of monoclinally north-dipping clastic sediments ranging in age from Late Cretaceous to Holocene. This sediment wedge lies unconformably on the Proterozoic basement and has a non-uniform thickness throughout the basin (Figure 2.2). From south to north this sedimentary package increases in thickness. Also a westward increase can be noted. According to Wong (1989) the thickness varies between 200 m in the east and 2000 m in the west.

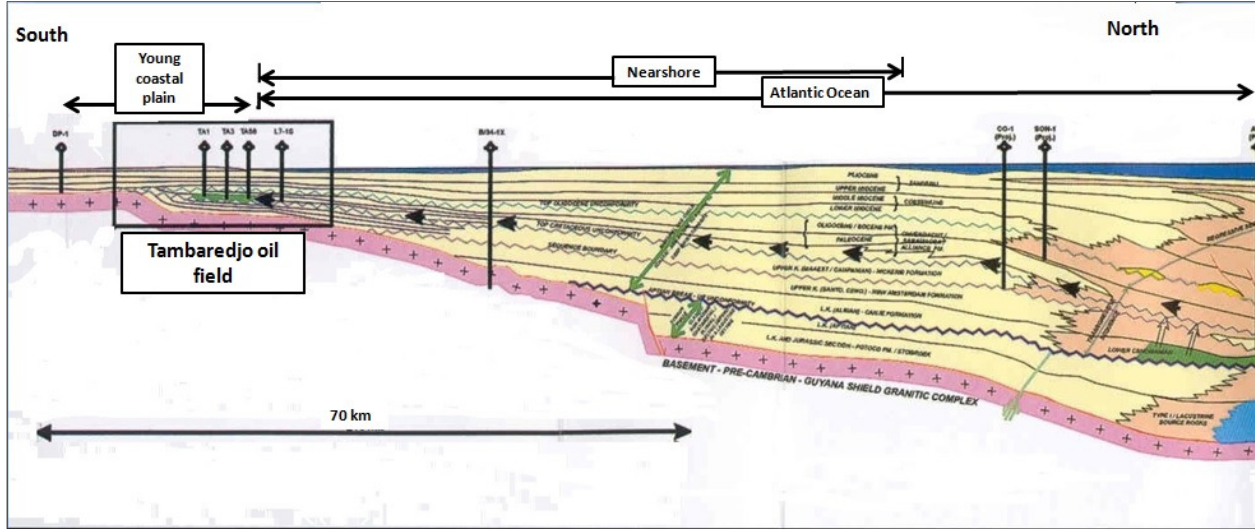


**Figure 2.2:** N-S Cross-section from the Guyana Shield to the Atlantic Ocean showing the Corantijn Group and the location of the Tambaredjo field.(modified, courtesy of Staatsolie Maatschappij Suriname N.V.).

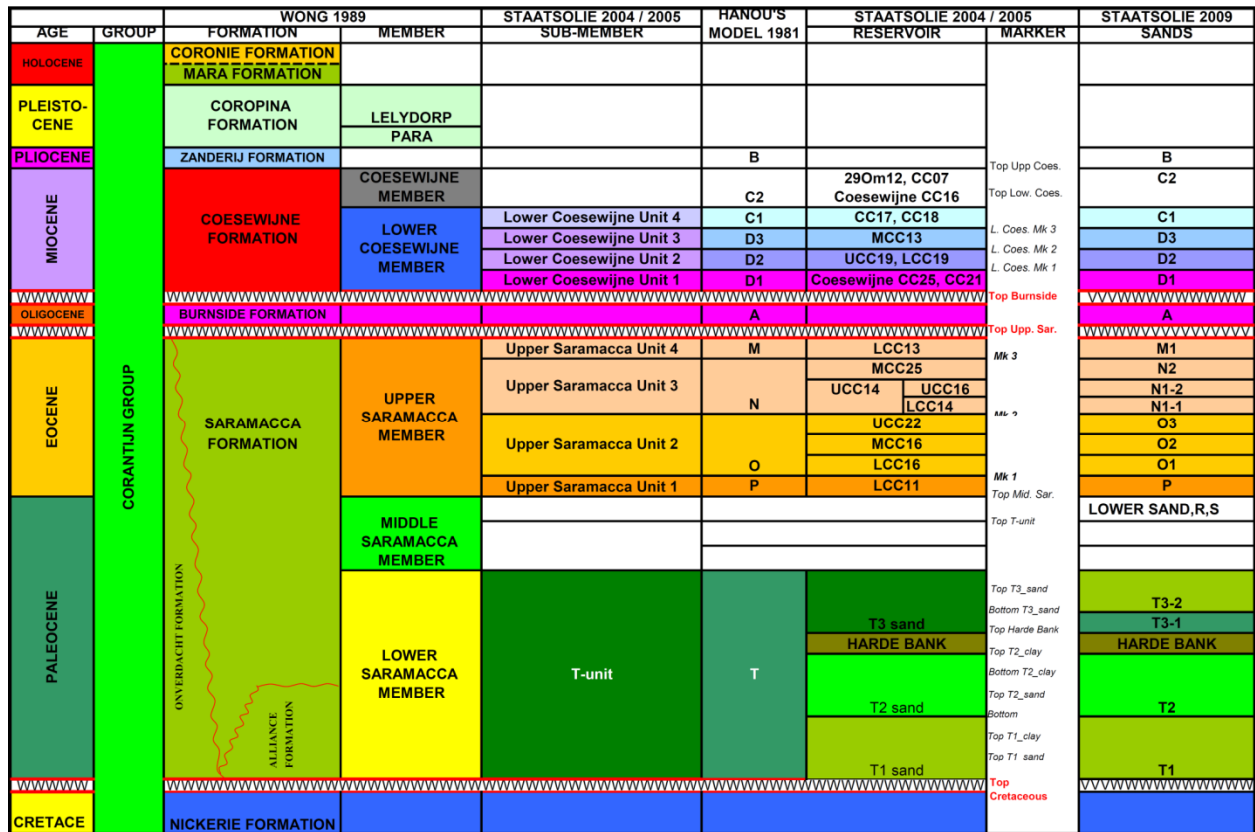


Figure 2.3: Stratigraphic column onshore Suriname with different stratigraphic markers and reservoir units within the Tambaredjo oil field (Courtesy of Staatsolie Maatschappij Suriname N.V.)

The sediments of the onshore Cretaceous interval are part of the Nickerie Formation, the oldest Formation within the Corantijn Group (Figure 2.3). According to Van Strien (2010) the formation has a Cenomanian to Maastrichtian age and can be divided into a lower and upper part. The Lower Nickerie Formation has a Cenomanian to Santonian age and the sediments within this formation onlap the Proterozoic basement. This formation is separated from the upper Nickerie formation of Campanian to Maastrichtian age by a regional unconformity. The Nickerie formation is characterized by a regular alternation of consolidated and unconsolidated quartz sands with multi-coloured claystones, siltstones and minor shales (Wong, 1989). As one of the first authors, Van Strien (2010) was able to create a sequence stratigraphic framework for the Cretaceous Nickerie Formation. His study resulted into the identification of six members within the Nickerie Formation. The Lower Nickerie Formation as well as the Upper Nickerie Formation contains three members. In the next sections these members are explained briefly.

## **2.2.1 Lower Nickerie Formation**

### ***Member 1***

The sediments of this member were deposited as prograding alluvial and fluvial deposits on the Proterozoic basement. The depositional environment is highly variable. From high gamma ray values, it was suggested that a base level rise occurred, which flooded the basin. During the flooding lignites were deposited. At the same time, coarse-grained material was deposited from local sources. There is also an indication that radioactive sands might have been deposited.

### ***Member 2***

After the base-level rise, a base-level fall occurred. This base level-fall forms the lower sequence boundary of Member 2. The sands in this interval are shallow braided rivers deposits and alluvial fans, lying further inland. The deposits are characterized by high Th/K spikes suggesting a mainly continental depositional environment. From high gamma ray values it was suggested that the sand intervals in this member are interbedded by either shales or radioactive sands.

### ***Member 3***

This Member is interpreted as the first fully fluvial system of the Lower Nickerie Formation. The lower boundary of this formation is the sudden drop in high Th/K gamma ray values. The sands in this interval are clean, well-connected sands which seem to have been deposited on a flat coastal plain during a base level rise. Although a transgression might have occurred during deposition of this member, no widespread deposits of shale have been found.

## **2.2.2 Upper Nickerie Formation**

The Upper Nickerie Formation is separated by the Lower Nickerie Formation by an unconformity at the top of the Lower Nickerie Formation, corresponding to a period of non-deposition and erosion. The sediments of this interval are characterized by fluvial and upper delta plain deposits comprising of clinofolds and aggradational facies. Van Strien (2010) subdivided this section into three sequences: Member 4, 5 and 6.

### ***Member 4***

This member is associated with a large transgression, which can be seen as an onlap and downlap onto the boundary between the Lower and Upper Nicker Formation. The

transgression occurred without widely deposition of shales. This member can be characterized by low Th/K, differentiating it from the lower members. This is also the first member showing distinct clinofolds associated with an offlap break and progradation in a deeper sea.

#### ***Member 5***

The basal sands of this member represent clean sands, with generally low gamma ray values, deposited in incised valleys or confined channels. Occasionally there are thick shales on top of the sandbeds with occasionally interbedded sands. In some areas the interval has continuously stacked fining upward sandbeds. Low Th/K values, indicating less kaolinization, and clinofolds can also be seen in this member. Deposition occurred during lowering of the base-level, which may have induced incision. As the base level dropped the shelf prograded seaward.

#### ***Member 6***

The lithologies present in Member 6 are similar to Member 5. The shale is thinner than and not as widespread as in Member 5. Individual sandbeds may also show fining upward trends and could have been deposited as point bars on a flattened coastal plain. The depositional environment is the same as Member 5, with further seaward progradation of the shelf.

### **1.1.1 2.2.3 Upper Cretaceous unconformity (Cretaceous-Tertiary Boundary)**

In the Tambaredjo area the Palaeocene to Eocene sediments, called the Saramacca Formation, unconformably overly the Upper Nickerie Formation (Figure 2.3). This unconformity is formed due to a major regression during the Late Cretaceous- Early Palaeocene period. On the density log there is a sudden increase in density at the Cretaceous- Tertiary boundary (Nandlal & Arnon ,1998). This sudden increase is due to the more cemented and compacted sediments of the Cretaceous. The uppermost Cretaceous sediments are also strongly kaolinized. Wong (1989) mentions that the sands of the Cretaceous Nickerie Formation could be differentiated from younger formations by the weathered surfaces of the grains and the occurrence of orange and reddish brown quartz grains. From well data of the Tambaredjo field it is known that the weathered surface of the Cretaceous unconformity consists of a grey to white, firm to hard kaolinitic sandy clay. In some wells the unconformity is not present and the Palaeocene T-sands, directly overly the reworked Cretaceous sediments. Nanlal & Arnon (1998) further state that the weathered surface effectively seals off Cretaceous fluids from the overlying T-sands.

### **2.3 Faults below the Tambaredjo oil field**

In the Tambaredjo field area, Kisoensingh (2009) has identified several fault patterns (Figure 2.4). These fault patterns have EW, ENE-WSW, NE-SW and NS trends. The EW and ENE-WSW fault patterns are transcurrent faults formed during the Late Cretaceous due to rifting of the South American and African plates. The EW fault patterns run through the whole Tambaredjo area. From the Precambrian till the end of the Cretaceous, the faults have a constant offset, indicating pre-faulting sediments. At the end of the Cretaceous normal faulting started which most likely lasted till the Late Palaeocene. Afterwards reverse movements occurred lasting till the end of the Miocene.

The ENE-WSW fault pattern, also known as the 'Broederschapsbreuk', is as the EW trending faults a strike slip fault. According to Kisoensingh (2009), were these faults active from the Precambrian till the end of the Palaeocene. During the Upper Cretaceous till the Early Palaeocene these faults had more or less no vertical displacement. However, during the Late Palaeocene they showed a decreasing vertical displacement until the faulting ceased.

The NE-SW trending faults are normal faults, which were active faults during the Late Cretaceous until the end of the Palaeocene. However due to its close location to the EW trending faults, Kisoensingh (2009) could not determine its displacements during this interval.

During the Late Triassic a series of mafic dykes intruded the Proterozoic basement. This caused weaknesses in the basement eventually leading to the initial break-up of Gondwana. These weaknesses were reactivated in the Late Cretaceous to Tertiary times and led to the NS trending faults visible in the Tambaredjo oil field.

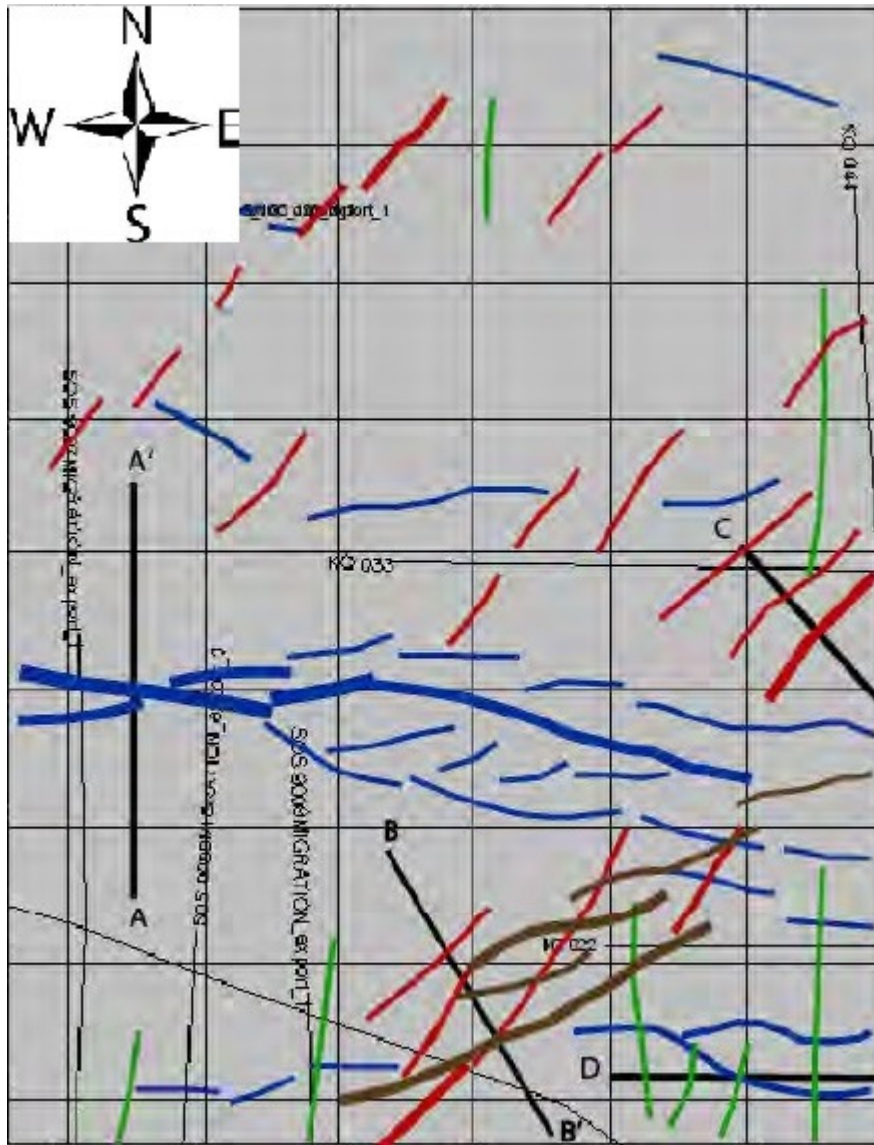


**Figure 2.4:** Faults identified in the 3D seismic area. The different colours represent different fault patterns identified. Blue lines→ EW trending faults, Red lines→ NE-SW trending faults, brown lines→ ENE-WSW trending faults and green→ NS trending faults. Imaged modified from Kisoensingh (2009).

## **3 Seismic Attributes**

### **3.1 Introduction**

Since 1970, seismic attributes have been developed and now they are considered to have a major part in seismic interpretation. Seismic attributes are computed or implied quantities from seismic data. They consist of quantities such as interval velocity, reflection terminations, AVO and as well complex-trace attributes. Seismic attributes are considered to have a relationship with the lithological and petrophysical properties of the imaged rock units.

Before calculating seismic attributes, seismic data needs to be optimally processed, meaning that any or all noise should be eliminated from the seismic data. Noise can occur randomly, but it can also be related to acquisition or even as processing artifacts (Chopra & Marfurt, 2007). Noise can decrease the signal-to-noise ratio and as a result can distort horizon or fault interpretation. Removing noise can be done in post stack processing (Chehrizi et al. 2013). After the calculation of attributes it is suggested to calibrate the attributes with well data to verify whether the features shown on the attribute maps are real or artefacts. This will thus give a better interpretation of attribute maps (Hesthammer et al. 2001).

There are great amount of attributes available, but not all of them are useful in all cases. When doing a seismic attribute analysis we thus need to use appropriate attributes. Several authors (Raeesi et al (2012), Pigott et al (2012), Xian et al. (2013)) have agreed on the principle of selecting the right attributes. According to them seismic attributes must have a geological meaning and should thus be able to imply variations in facies, lithologies or physical properties. Further Chopra and Marfurt (2007) state each attribute should only measure one property of the seismic response. In that way multiple attributes can be combined graphically or numerically, for example through neural networks, to give a better interpretation of the seismic data.

### **3.2 Classification of attributes**

Many authors have tried to classify the seismic attributes into families. One of the classifications is dividing attributes based on the relationship to geology. The attributes can thus be divided into geometrical and physical attributes. Geometrical attributes enhance the visibility of events and their spatial relationships and may be thus used to identify depositional patterns and features related to lithology. Physical attributes are directly related

to physical parameters of the subsurface (Subrahmanyam & Rao, 2008). For example the magnitude of a peak of an envelope depends on the acoustic impedance contrast of a bed (Taner 1992; Taner, 2001).

Another classification of attributes is based onto their computational characteristics. The attributes can be divided into Instantaneous attributes and wavelet attributes. The calculation of instantaneous attributes proceeds sample by sample, which thus shows instantaneous variations of various parameters. The instantaneous attributes reflection strength, instantaneous phase and frequency are calculated from a complex trace. A complex trace is a seismic trace consisting of a real and an imaginary part. The real part is the actual seismic trace and the imaginary part is the Hilbert transform of the real seismic trace. The real trace and the quadrature trace share the same amplitude, but the quadrature trace has a phase rotation of 90 degrees (Figure 3.1). With this phase rotation, zero-crossings on the real trace coincide with peaks on the quadrature trace and also vice versa.

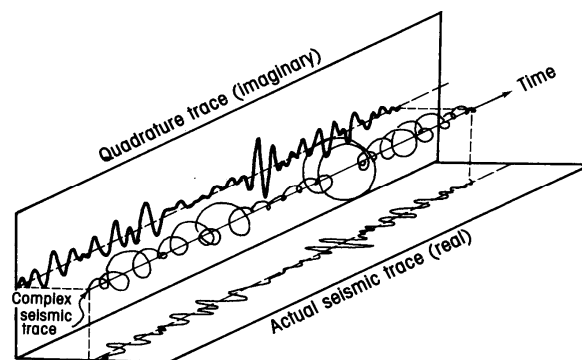


**Figure 3.2:** Sketch of an actual seismic trace and its Hilbert transform, quadrature seismic trace (Taner (1992))

Wavelet attributes on the other hand comprises the instantaneous attributes measured at the peak of an envelope, between two adjacent envelope minima. Computation of the wavelet attributes takes place at the peak of the envelope, because most of the signal energy originates from the vicinity of the envelope peaks (Chopra & Marfurt, 2005).

Pre-stack and post-stack attributes are a method of classifying the attributes based on their domain. Pre-stack attributes work with Common Depth Point (CDP) or image gather traces, which contain directional (azimuth) and offset related information. Pre-stack attributes are useful for getting information regarding fluid content and fracture orientation. The main disadvantage of pre-stack attributes is that it produces huge amounts of data, which results in higher computation time (Taner, 2001).

Post-stack attributes work with stacked and migrated seismic sections. Stacking is an averaging process, where traces have been added together to reduce the noise level and

increase the overall data quality. A disadvantage of stacking is that it eliminates offset and azimuth related information. Migration is a process where seismic events are re-located to their true subsurface positions. Migration can either be in time or in depth. Time migration is applied in the time domain, meaning that temporal variables, such as frequency, maintain their physical dimension. However in depth migration, frequency is changed to wave number, which is a function of propagation velocity and frequency.

<p>Physical Attributes</p> <ul style="list-style-type: none"> <li>• Amplitude Envelope</li> <li>• Frequency and Phase</li> <li>• Spectral Decomposition</li> <li>• Instantaneous Amplitude</li> </ul>	<p>Geometrical Attributes</p> <ul style="list-style-type: none"> <li>• Coherence</li> <li>• Variance</li> <li>• Dip</li> <li>• Azimuth</li> <li>• Discontinuity</li> </ul>
<p>Post-Stack Attributes</p> <ul style="list-style-type: none"> <li>• Reflection Strength</li> <li>• Envelope Derivative</li> <li>• Instantaneous Phase</li> <li>• Cosine of Instantaneous Phase</li> <li>• Instantaneous Frequency</li> <li>• Instantaneous Q</li> <li>• Relative Acoustic Impedance</li> <li>• Thin bed indicator</li> </ul>	<p>Pre-Stack Attributes</p> <ul style="list-style-type: none"> <li>• RMS velocity</li> </ul>

**Table 3.1:** Classification of seismic attributes

**3.3 Attribute Analysis in Clastic Depositional Systems**

A depositional system is defined as a three-dimensional body of sediment deposited in an environment governed by interrelationships of physical, chemical, or biological processes. Some examples of clastic depositional systems are alluvial fan, fluvial, delta, eolian and lacustrine systems (Galloway & Hobday 1996). Referring to the second chapter, it can be

concluded that the Suriname-Guiana basin can be defined as a fluvio-deltaic and coastal clastic depositional system.

Pigott et al. (2012) have identified some useful attributes for identifying seismic facies and their changes in clastic depositional systems. Seismic facies can be described as the appearance of underlying geological facies or structural features in seismic data, such as clinofolds, bed continuity, hydrocarbon indicators, faults and fractures. Seismic facies changes can thus be seen as any change in seismic character, for example amplitude, frequency, phase and geometry (Raeesi et al. 2012). According to Pigott et al. (2012) the attributes effective in delineating seismic facies are Amplitude Envelope, Chaos, Cosine of Phase, Dip Deviation, Instantaneous Frequency, Instantaneous Q factor, Relative Acoustic Impedance and Variance.

One of the objectives of this study was to find geological features from seismic attribute analysis in the Cretaceous below the Tambaredjo field. One of the most important features for hydrocarbon exploration in a clastic depositional system is channels. They are one of the main locations where hydrocarbons are accumulated (Zhang et al., 2011). To improve the drilling accuracy it is thus important to adequately identify channel bodies and their boundaries. However, identifying channels can be difficult. One of the problems is that their thickness often falls below the vertical seismic resolution range (smaller than a quarter of the seismic wavelength). This causes the reflections from the top and bottom interface to interfere with each other, which results in difficulties in separating these interfaces in the time domain. Channels also frequently change their course and position over time, which implies a strong lateral heterogeneity of channel sand bodies. Coupled with significant erosion, they are intercrossed and occasionally cut in by faults (Sun et al., 2010; Zhang et al., 2011).

Several authors have suggested the coherence attribute as an effective attribute to identify channels and other geological features such as faults, dikes and deltas (Liu & Marfurt, 2007; Zhang et al., 2011; Rezvandehy et al., 2011). Sometimes channels are also recognizable from their high seismic amplitudes, thus amplitude detection attributes might also be applicable (Zhang et al. 2011). Zhang et al. (2011) also found the instantaneous and energy attribute sensitive to channel features. However, sometimes these identification methods are only effective for large and continuous channels. For smaller channels, below thin bed resolution, they are not adequate. Take for example the coherency attribute: As a channel becomes thinner (smaller than one-quarter wavelength), their waveform becomes constant and the coherence calculation based on the waveform shape is thus not able to delineate the channel at

all (Liu and Marfurt, 2007). According to some authors, spectral decomposition can also be used as an effective attribute to highlight thin beds (Rezvandehy et al. 2011; Liu & Marfurt 2007; Chopra & Marfurt 2008; Zhang et al. 2011). Thin beds have a special relation with frequency. If a layer thickness decreases, the peak frequency increases (Sun et al. 2010). The peak frequency is defined as the frequency corresponding to the maximum or peak amplitude of a bed. In order to map thin beds, Rezvandehy et al. (2011) use the instantaneous amplitude attribute, which is directly related to acoustic impedance differences, to get the peak amplitude of a known thin layer. After retrieving the amplitude, it is Fourier transformed which results in the frequency of the peak amplitude. It is thus possible to use the achieved frequency in a spectral decomposition to find other thin bed layers.

Another method to show thin beds is with the seismic attribute introduced by Sun et al. (2010). This attribute, named thin bed indicator, is calculated as the ratio of the peak frequency and peak amplitude, and is used to indicate channel thicknesses. Both frequency as well as amplitude are separately related to a channel thickness. Peak amplitude increases with increasing thickness and decreases with layer thickness, whereas frequencies increase with decreasing thicknesses below the tuning thickness. Sun et al. (2010) find that combining peak frequency and peak amplitude in to a new attribute gives a better prediction of channel thickness and thus in their study thin channels could be identified.

Zhang et al. (2011) also suggest to use RGB technology to image smaller channels and other tiny structures such as faults. RGB technology displays multi attributes in one window against red, green and blue primary colours (Chopra & Marfurt, 2008). Zhang et al. (2011) finds that this is an effective method to gain more information from all the attributes compared to a display of one attribute, which contains limited geological information. From their experience combining, coherence, instantaneous and energy-half time attributes in a RGB display makes these attributes even more effective. Generally channels have frequencies ranging from 5 – 45 Hz and some researchers have used the RGB technology to plot spectral components of three different frequencies within the before mentioned bandwidth for a better delineation of channels (Chopra & Marfurt 2008; Zhang et al. 2011)

Apart from mapping geological features, the other objective of this study is to predict lithofacies and their distribution within the survey. Many authors suggest to use multi attribute analysis in predicting lithofacies (Raeesi et al., 2012; Kuroda et al. ,2012). The basic workflow suggested by Raeesi et al. (2012) is selecting appropriate attributes based on their abilities to reveal geological properties. Then these attributes are used as an input for a multi-

attribute analysis such as an Artificial Neural Network (ANN). Artificial Neural Networks (ANNs) are information processing systems inspired by the abilities of the human brain. Some of these abilities are processing data in a parallel structure, learning from observations, extracting information from a large amount of input data and working with inconsistent and noise contaminated data. ANNs can be trained to find any arbitrary nonlinear input-output relationship within a specific data set (Zhang et al. 2003). To find these non-linear relationships or patterns, two approaches may be recognized, supervised and unsupervised training.

In an unsupervised analysis seismic data is grouped into areas with distinct seismic behaviour without the use of well data. These results in a heterogeneity map showing different classes that might be related to different lithofacies or reservoir properties. But these classes are not labelled. In a supervised training, classes are shown with each class representing a known lithology, lithofacies or reservoir property based on, for example, core analysis. For this a given parameter such as lithology, lithofacies or reservoir property has to be captured by a set of seismic attributes and it has to be calibrated by well data. With this information as input to an ANN several similar parameters can be found in the survey area (Raeesi et al. 2012).

### **3.4 Evaluation of Attributes**

In this chapter the attributes used in this study will be described regarding their properties and their abilities to discern certain features. Based on the literature review on seismic attributes and referring to the advice given in chapter 3.1 on choosing appropriate attributes, a selection of the following instantaneous and wavelet attributes were made:

- Instantaneous attributes: instantaneous amplitude, cosine of instantaneous phase, instantaneous frequency, instantaneous Q factor, thin bed indicator
- Wavelet attributes: RMS energy, similarity, variance, spectral decomposition.

It can be noted that not all of the attributes suggested in the previous chapter are used. This is due to the fact that some attributes were not available in OpendTect and because of a short amount of time not all the attributes suggested could be evaluated. Important as well is to note that even though variance and similarity attribute measure more or less the same seismic property, they were chosen to enhance the seismic interpretation of faults. According to de Rooij & Tingdahl (2002) fault interpretation can be quite ambiguous so using more attributes might be useful for fault detection. RMS energy and instantaneous amplitude as well measure

the same seismic property, namely the amplitude, but the reason for selecting both attributes will be explained in the next chapter.

### 3.4.1 Instantaneous Amplitude

The Instantaneous Amplitude attribute is a physical attribute and it delineates areas of low and high amplitude. This attribute can be used as an aid in stratigraphic and structural interpretation to get information such as the change in acoustic impedance and reflection coefficients (Kuroda et al. 2012). According to Veeken (2007) the higher the velocity-density contrast, the higher the amplitude. Thus amplitude information might be used for indicating bright spots and major changes in lithology and the depositional environment (Taner, 1992; Shi et al., 2012). In their research, Kuroda et al. (2012) found that usually high values of instantaneous amplitudes were related to sandstones and lower values to mudstones. However, Veeken (2007) warns to be careful during interpretation. Sand and shales may exhibit similar acoustic impedance values. This can occur as a result of compaction, pore fluid content and porosity. Compaction increases the density of a rock, which in turn results in an increase in velocity. Amplitude information might also be used for identifying thin beds. Due to wave interference, the amplitude shows variations (Veeken, 2007).

The instantaneous amplitude is calculated as the modulus of the complex function  $F(t)$  (Eq. 1). In this equation  $f(t)$  represents the real trace and  $g(t)$  the Hilbert transform of the real trace (Taner, 1992).

$$F(t) = f(t) + i g(t) \quad (Eq. 1)$$

$$A(t) = \sqrt{f(t)^2 + g(t)^2} \quad (Eq. 2)$$

The values of this attribute vary between 0 and the value corresponding to the maximum amplitude. As indicate on Eq. 2, the instantaneous amplitude is independent of phase and thus directly relates to acoustic impedance contrasts.

### 3.4.2 Cosine of Instantaneous Phase

The Cosine of Instantaneous Phase is also known as Normalized Amplitude. As the name already implies it is calculated by taking the cosine of the instantaneous phase. For a clearer

picture, the instantaneous phase will be explained first and then the difference between cosine of instantaneous phase and instantaneous phase will be clarified.

The instantaneous phase Eq. 3) is calculated as the argument of the complex function in equation 1.

$$Ph(x, t) = \arctan \left[ \frac{g(x, t)}{f(x, t)} \right] \text{ Eq. (3)}$$

This attribute contains no amplitude information, but is rather associated with the phase propagation of a seismic wave front. Since a seismic wave front is by definition a line of constant phase, it can be assumed that at reflection boundaries the phase changes and thus the phase information can be used to identify geometrical shapes (Shi et al. 2012). A zero phase wavelet has a value of zero at a peak,  $180^\circ$  at a trough and  $90^\circ$  and  $-90^\circ$  for zero crossing. The phase values  $-180^\circ$  and  $180^\circ$  are equal and therefore, the instantaneous phase should be displayed with a circular colorbar (Halliburton, 2013). It is assumed that a value of zero corresponds to a peak, in SEG convention that would correspond to a down going increase of acoustic impedance. A phase value of  $180^\circ$ , which corresponds to a trough, indicates a decrease in acoustic impedance according to SEG polarity convention (Appendix A).

Kuroda et al.(2012) state that the instantaneous phase attribute highlights the continuity of reflectors and improves the intra-event signals. According to Taner (1992) it is also able to show the bedding configuration in more detail. This attribute is thus a geometrical attribute. The main difference between the cosine of instantaneous phase and the instantaneous phase is that the discontinuity at  $180^\circ$  and  $-180^\circ$  is removed. By taking the cosine of the instantaneous phase, the values vary between -1 and 1, where the value one stands for a phase value of zero, thus a peak on a seismic trace, and minus one for a phase value of  $-180^\circ$  and  $180^\circ$ , corresponding to a trough .

### 3.4.3 Instantaneous frequency

The instantaneous frequency is calculated as the time rate of change of phase (Taner 1992). However at  $2\pi$  jumps, the phase function is multi-valued and to avoid this problem the time derivative of the arc tangent function is taken (Eq. 4):

$$Freq(x, t) = \frac{\partial \arctan[g(x, t)/f(x, t)]}{\partial t} = \frac{\left[ f(x, t) \cdot \frac{dg}{dt} - g(x, t) \cdot \frac{df}{dt} \right]}{[f(x, t)^2 + g(x, t)^2]} \text{ (Eq. 4)}$$

According to Taner (1992) the instantaneous frequency attribute is an important attribute for interpretation. Taner (1992) states that this attribute can be used as a thin bed indicator. Low frequencies might be assigned to sand-rich layers and higher frequencies to shale layers. In an attribute map, interface interference associated to thin beds might be displayed as unusual values of frequencies with high fluctuations. The instantaneous frequency attribute can also be used to delineate low frequency fracture zones. Furthermore It might also highlight chaotic reflection zones due to excessive scattering. Pigott et al. (2013) state that instantaneous frequencies have many interpretation possibilities, the interpretations related to this attribute need to be geologically constrained. The many interpretation possibilities can be implied from looking at the general wave equation:  $v = f\lambda$  (  $v$ = velocity,  $f$ =frequency, and  $\lambda$ =wavelength. For example if thicknesses are constant (stable lambda), lower frequencies might imply slower rock matrix velocities and/or higher gas content in pores. Lower frequencies can also be attributed to possible fractured zones (Kuroda et al. 2012; Pigott et al. 2013).

#### **3.4.4 Instantaneous Q factor (quality factor)**

This attribute is a physical attribute and has a strong connection to porosity, permeability and fracturing (Taner, 1992). The Instantaneous Quality attributes represents the decay rate of the reflection strength, which might indicate changes in absorption. High Q factor values indicates low absorption and low quality indicates high absorption. For example, if different layers are visible on the seismic section and the instantaneous Q factor has different values, it is suggested that different lithologies are present (Pigott et al. 2013). Mathematically (Barnes 1993) defines the instantaneous Q factor as the ratio of the instantaneous frequency to twice the bandwidth. Looking at equation 5,  $q(t)$  is the quality factor,  $freq(t)$  the instantaneous frequency and  $decay(t)$  as the instantaneous decay rate:

$$q(t) = -\pi \cdot \frac{freq(t)}{decay(t)} \quad (Eq. 5)$$

According to Barnes (1993) the instantaneous decay rate is defined as the derivative of the instantaneous amplitude divided by the amplitude. Apart from a factor of  $2\pi$  and the fact that

the decay rate can be negative, the decay rate is equal to the instantaneous bandwidth, which is defined as the rate of relative amplitude change.

### **3.4.5 Variance**

The Variance attribute is also used for edge detection. It calculates the difference from a mean value and is used for indicating reflector discontinuities. However, it cannot be used to indicate reflector continuity. It returns high values for example at channel boundaries, faults, boundaries of an intrusive body and where channel downcutting takes place (Pigott et al. 2013).

### **3.4.6 RMS Energy**

This attribute can be defined as the average amount of energy within a specified time gate. It is calculated as the squared sum of sample values, within the time gate, divided by the number of samples. Higher values of RMS Energy are related to higher amplitudes. It is useful for identifying geological features as it enhances the lateral variations of seismic reflections.

### **3.4.7 Coherence and Similarity**

This attribute calculates the trace-to-trace match in both inline and crossline directions. A seismic waveform or trace is the product of a convolution of the seismic wavelet with the geology of the subsurface or earth response. If in any way the amplitude, frequency or phase changes, due to acoustic impedance contrasts and varying thicknesses of the layers, the waveform will change. Thus lateral varying acoustic impedances ,might give rise to lateral changes in waveform (Chopra and Marfurt, 2007).

There are some attributes measuring the coherency between trace segments. All of them are calculated differently, but require both dip and azimuth data for an adequate computation and a good interpretation of the results (Chopra and Marfurt, 2007). The similarity attribute in OpendTect is one of the attributes measuring coherency. It calculates the similarity between trace segments by one minus the distance between the trace segments-vectors, normalized by the sum of the vector's length (Eq. 6). A trace is represented by a vector. The components of a

vector are made of the samples of a trace. In equation 6, X and Y represent the vector's relating to different traces and N is defined as the number of samples in a trace.

The values of this attribute vary between 0 and 1, where the similarity value 1 represents completely identical traces in waveform and amplitude. A value of zero means that the traces are phase rotated by 180° (de Rooij & Tingdahl 2002). Fault planes are displayed as low coherency lines in an attribute slice and channels are displayed as high coherency zones (Zhang et al. 2011).

$$sim = 1 - \frac{\sqrt{\sum_{i=1}^N (X_i - Y_i)^2}}{\sqrt{\sum_{i=1}^N X_i^2 + \sum_{i=1}^N Y_i^2}} \quad (Eq. 6)$$

### 3.4.8 Thin Bed Indicator

The thin bed indicator in OpendTect is different than the one proposed by Sun et al. (2010). This attribute is calculated as the difference between the instantaneous frequency and the envelope weighted frequency, which is the instantaneous frequency weighted by the envelope over the given time window (Eq. 7).

$$thin\ bed(t) = \omega(t) - \bar{\omega}(t) \quad (Eq\ 7)$$

Sometimes the instantaneous frequency jumps or goes in reverse direction and thus large variations between the instantaneous frequency and the time-averaged frequency exist. This abnormal behaviour of the instantaneous frequency can be associated to interference of reflectors. Taner (1992) also finds that the thin bed indicator is indicative of non-reflecting zones, when it shows a lateral random or 'salt and pepper-like structure. He also noted that in case of a smooth variation in values, it is still unclear what happens. It might be related to bedding characteristics, but this has to be investigated further.

### **3.4.9 Spectral Decomposition**

Spectral decomposition is an attribute used to decompose seismic data, consisting of a normal frequency bandwidth, into discrete frequency intervals. Spectral decomposition is useful for delineating thin beds, as thin beds consist of a characteristic expression in frequency domain. Thinner beds are associated with higher frequencies, while thicker beds with lower frequencies (Brown, 2004).

## 4 Methodology

When doing a qualitative attribute analysis, the workflow usually consists of selecting appropriate attributes, computing them and using time slices, phantom-horizon slices or stratal slices to view features of interest. According to Chopra and Marfurt (2007), phantom-horizon slices are created by selecting a horizon and flattening the seismic data along this horizon. The slab of flattened data is then cut through with time slices. The disadvantage of using this is that the horizon slices might cut to formations with different geological ages, because reflections or sequence boundaries are usually not parallel to each other. An alternative is to use stratal slices. Stratal slices are created as intermediate horizons in an interval between two sequence boundaries. They are produced in such a manner that they are proportional between the sequence boundaries and correspond to a single geologic time.

In this study, chronostratigraphic slices similar to the strata sliced defined by Chopra and Marfurt (2007) were used for interpreting attributes. The stratal slices were created from performing a Wheeler transform on a Horizon Cube in OpendTect, software developed by dGB Earth Sciences. Two important inputs for the Horizon cube were two picked horizons, which represent the bounding surfaces of the Horizon Cube, and a steering cube. The following chapters describe the several steps and their partial products in the workflow.

### 4.1 Steering cube

The first step in the workflow was the generation of a steering cube. The steering cube is a volume containing the dip and azimuth information at every sample location of seismic events. The steering cube is for example necessary for calculating attributes. The efficiency of some seismic attributes can be enhanced by calculating the attributes in the direction of local dip and azimuth. Take for example the calculation of the similarity attribute in a dipping environment. As known from the previous chapter, the similarity attribute estimates the differences between traces. If there is no dip data available, the attribute would give incorrect results. It is thus necessary to have directional data. This data can be delivered by a steering cube. Calculating the steering cube basically scans the seismic volume for dips, follows dips trace by trace (this process is called steering) and saves the directional data in the steering cube (Chehrazi et al. 2013).

To improve the steering cube, the steering data was filtered by a dip-steered median filter. This process reduces the random noise level and enhances the lateral continuity of seismic

reflectors. The term ‘dip-steered’ means that the process uses dip and azimuth information from seismic reflections. Whereas median filtering implies that the centre amplitude in a dip-steered circle, containing the seismic traces being scanned, is replaced by the median amplitude within the extraction circle. This results in smoothening of the seismic data.

## **4.2 Horizon Interpretation**

In this study one horizon has been interpreted, the Top of the Cretaceous. A second horizon was created by making an exact copy of the Top Cretaceous and shifting it 60 ms below the Top of the Cretaceous. This interval was thought suitable for an adequate Horizon Cube calculation. The Top Cretaceous horizon dips in the northern direction. The total dip over the seismic area is estimated to be approximately 160 ms in two-way-travel time (TWT).

The boundary between the Cretaceous and the overlying Palaeocene sediments is marked by a large shift in the density logs, which results in a hard kick or a downward increase in acoustic impedance. The 3D seismic data used in this study has a SEG polarity for zero phase wavelets. According to SEG polarity convention this means that a downward increase in acoustic impedance along an interface, such as the Top of Cretaceous, is displayed as a (blue) peak on seismic data. Even though the top Cretaceous is a hard kick, it is not easily distinguishable everywhere. Schram de Jong (2003) suggest two reasons for this. Either reworking of material, which causes a gradual density shift instead of a sharp density shift, or the occurrence of a high density calcareous clay layer lying directly on the Top Cretaceous Unconformity, which results in a small velocity-density contrasts.

To identify the Top of the Cretaceous assistance was obtained from geologists of Staatsolie Maatschappij Suriname N.V. However, the interpretation of the Top of Cretaceous was incorrect. The old 3D seismic data was displayed as having European polarity (Non-SEG) and according to this, the Top of Cretaceous was displayed as a red trough. This interpretation of the Top of Cretaceous was also used in the re-processed seismic data set and further also in this study. Thus, the Top of Cretaceous was picked at a trough instead of a peak. Due to a lack of time, the Top of Cretaceous could not be re-interpreted or calibrated with well data. However, this incorrect interpretation is not expected to have an effect on the results. All the attributes are still calculated in the Upper Cretaceous interval and by using wavelet attributes, one value is retrieved from a whole time window instead of one point in time. Therefore the RMS energy attribute was chosen in addition to the instantaneous amplitude, which retrieves amplitude information only at one point in the time interval.

### 4.3 Horizon cube

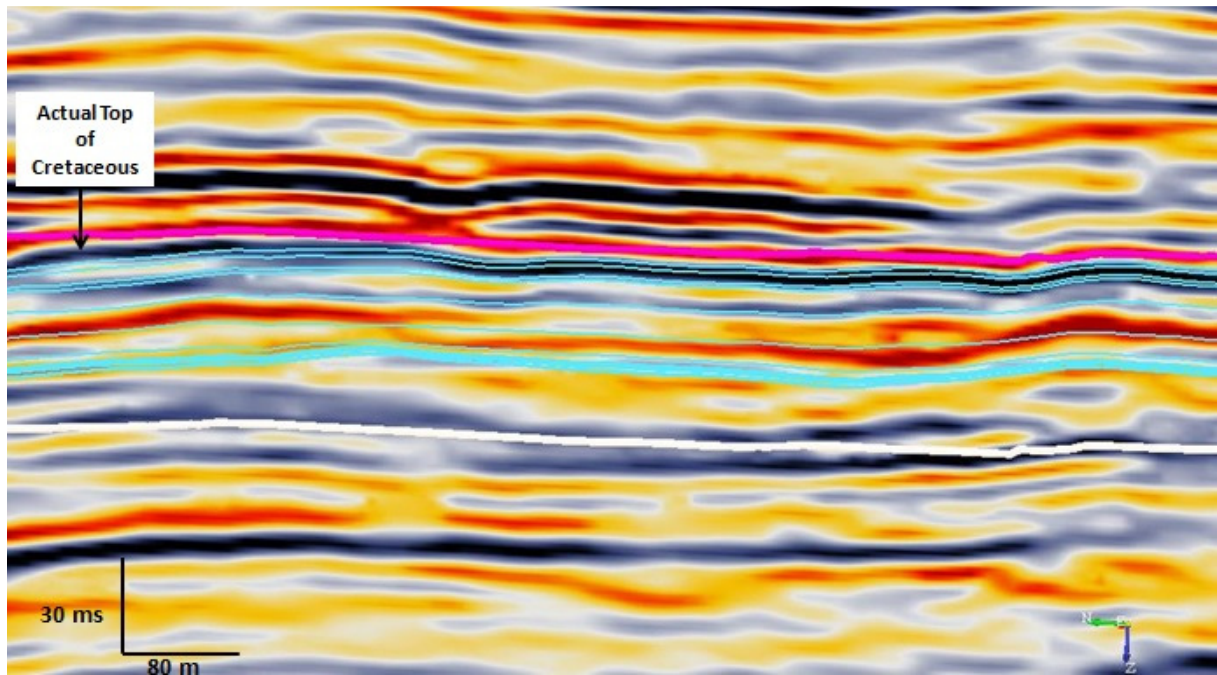
The Horizon Cube is a dense set of auto-tracked 3D horizons, whereby each horizon in the Horizon Cube corresponds to a (relative) geologic time (Qayyum et al., 2012). The two interpreted horizons were important for calculating the Horizon Cube, because they form the bounding surfaces of the Horizon Cube. Also the steering cube is an important input for the Horizon Cube. The dip and azimuth data enclosed in the steering cube is used for auto-tracking the horizons within the Horizon Cube. This form of auto-tracking is also known as Data driven method. The other method for creating a Horizon cube is the Model driven method. This method creates horizons by interpolating between the bounding surfaces or it adds horizons parallel to the bounding surfaces.

Figure 4.1 shows that between the two bounding horizons (Top Cretaceous and shifted top) there are intermediate horizons created in the 60 ms time interval. The parameters for the Horizon Cube were set such that the maximum gap between the intermediate horizons was set for 8ms. This implies that after every horizon, the next horizon generated would have a maximum gap of 8ms with the previous one. The horizon cube resulted in the generation of 14 intermediate horizons.

The top of the Cretaceous is a sequence boundary so it corresponds to one point in relative geological time and thus it can be defined as a chronostratigraphic horizon. Also all the other intermediate horizons created in the Horizon Cube can be classified as chronostratigraphic horizons as a first order approximation.

After creating the Horizon Cube, the chronostratigraphic horizons were flattened out by a Wheeler transform (Qayyum et al., 2012). Wheeler transform enables seismic interpreters to display seismic data and seismic attributes along flattened chronostratigraphic surfaces get a better understanding of the depositional history and the distribution of several lithofacies. These flattened surfaces can be defined as stratal slices, which were mentioned earlier.

Since the objective was to study an interval of about 20 m, which more or less corresponds to a TWT travel time of 20 ms (taking an average velocity of 2000 m/s), only the first four horizons (including the Top of Cretaceous) in the Horizon Cube were selected for displaying and calculating the attributes. The time interval between the Top of Cretaceous and the fourth intermediate horizon could not be estimated accurately because of its varying behaviour, but in average the time interval was around 25 ms.



**Figure 4.1:** Part of crossline 20 showing the Horizon cube (blue lines) with its bounding surfaces (pink and white line) and the 14 intermediate horizons created by a data driven method. The actual top of Cretaceous is also pointed out in this image.

#### 4.4 Seismic Attribute Analysis

In OpenTect there are two methods of calculating the seismic attributes. The attributes can be calculated on-the-fly, meaning that they are calculated on the foreground along a given horizon or time slice. After the calculation is finished, the attributes are displayed directly along the given horizon or slice. The other method is to calculate them in the background. Here the calculated attributes are stored in a volume and afterwards they are loaded onto a horizon or slice of interest. All the attributes in this study were calculated in the background. After calculation the stored attribute data had to be converted to the Wheeler domain, where the attributes could be displayed along flattened stratal slices.

#### 4.5. Combination of seismic attributes

As mentioned before by Chopra and Marfurt (2007), combining attributes numerically and graphically can give a better interpretation of seismic data. To enhance the interpretation in this study, both RGB displays as well as an unsupervised Artificial Neural Network (ANN) were used. These combination of attributes, were all performed or calculated on the Top of the Cretaceous.

Following Zhang et al. (2011), Brown (2004) and Rezvandehy et al. (2011), RGB technology was used in order to delineate smaller structural and stratigraphic structures such as thin beds

and small faults. The RGB technology was used for the spectral decomposition attribute, where the retrieved images of the 15, 30 and 45 Hz, were blended into one display. Furthermore a blending of the instantaneous amplitude, similarity and instantaneous phase was performed.

In order to give an indication of the distribution of different lithologies or lithofacies, an unsupervised ANN was performed. This was done by an unsupervised Vector Quantiser (UVQ). The UVQ uses either the seismic waveform or attribute information and groups or segments this data into different classes (Rabelo ,2006). The number of these classes can already be given at the start of the segmentation. Because RMS energy, instantaneous phase and instantaneous frequency were one of the most effective attributes, they were used as input for the UVQ segmentation. The number of classes was defined according to Wong (1989) and Van Strien (2010).They state that the onshore Cretaceous interval, Nickerie Formation, consists of five different lithologies, sands, claystones, siltstones, shales and lignites.

## 5 Results and Discussion

After all the calculation of the attributes, this is the final step in an attribute analysis. In this chapter the stratal slices will be analysed in order to find geological features of interest, acquire a better understanding of the geology and predicting lithofacies and their distribution within this area. Please note that the width and length of all the slices shown in this chapter have a width and length of respectively 8 and 10.4 kilometres, which corresponds to the dimensions of the 3D survey area.

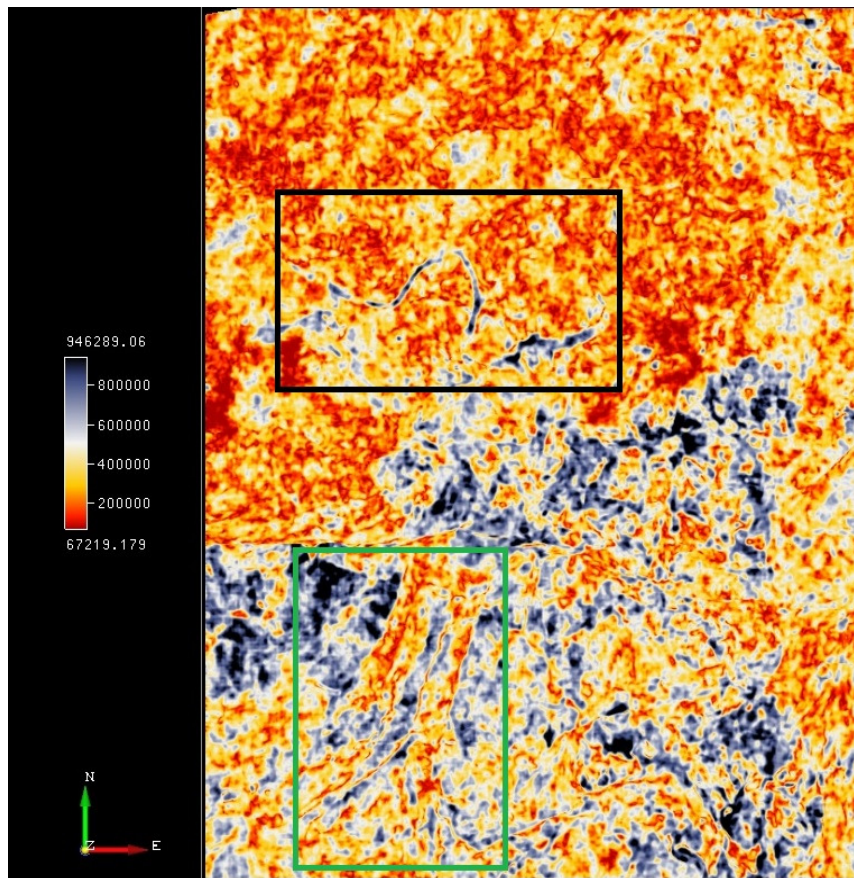


**Figure 5.1:** Instantaneous amplitude stratal slice of the Top Cretaceous. The black rectangle delineates an ESE-NNW trending channel feature, whereas the green rectangle encloses a linear NE-SW structure. Please note that the width and length of the slice correspond to the dimensions of the survey area. The width is 8 kilometers and the length 10.4 kilometers. These dimensions are valid for all the slices shown in this chapter.

From the instantaneous amplitude stratal slice of the Top of Cretaceous (Fig 5.1) some noteworthy features can be depicted. First of all in the northwest section there is a channel feature clearly distinguished. This feature is marked by high amplitudes, high channel sinuosity and an ESE-NNW trend. More southward of the channel a linear NE-SW structure can be delineated. This structure alternates in low and high amplitude values. From figure 5.1

it can also be noted that high amplitude values are seen more in the south, whereas the northern section correspond to lower amplitude values.

Looking at the similarity stratal slice in the left image of figure 5.2, the channel feature is also clearly distinguishable (displayed in the red rectangle). The channel corresponds to high coherency values which are displayed in light grey colour. Low coherency values, such as faults, are displayed in black. The width of this channel feature is approximately around 40-75 meters. From its high coherency and amplitude values, it is likely that this feature is a sand prone channel (Kuroda et al., 2012; Zhang et al., 2011).

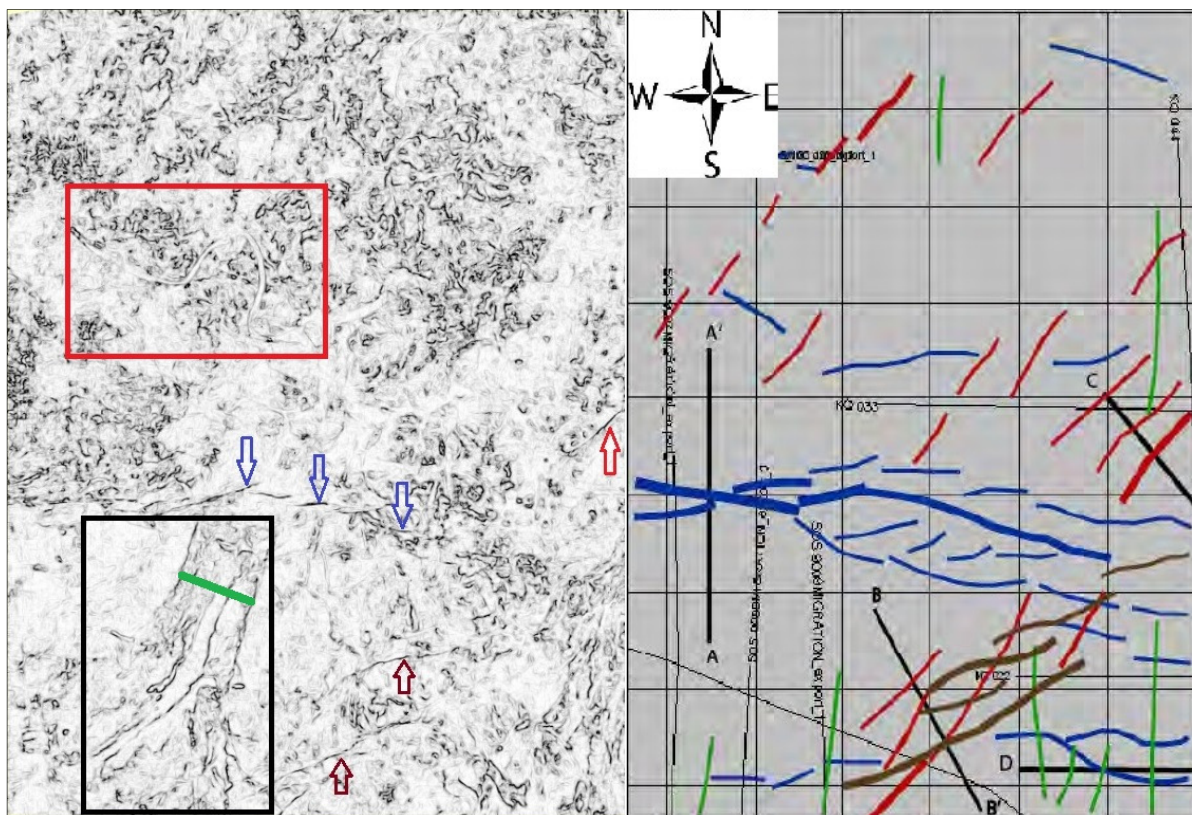


**Figure 5.2:** Similarity stratal slice (left) and fault map of the Tambaredjo 3D area (right) (modified from Kisoensingh, 2009). On the left image, red box delineates the channel feature; black square delineates the linear structure. Further arrows indicate different faults. Blue arrow → EW trending fault system, red arrow → NE-SW trending fault and brown arrow → broederschapsbreuk.

Comparing the images in figure 5.2, it can be seen that faults recognizable on the similarity slice correspond to faults mentioned by Kisoensingh (2009). The blue arrows in the similarity slice highlight the EW trending fault system seen in blue colours on the right image. Similarly, the brown arrows mark the Broederschapsbreuk seen in brown colour on the right image. Further a NE-SW trending fault is also pointed out by a red arrow on the left image.

Also seen from the similarity slice in figure 5.2, is the linear structure that was seen before in the instantaneous amplitude slice. Here the linear structure is imaged better. The width of the structure, marked by a green line in figure 5.2, is roughly estimated to be around 800 – 1000 meters. The question is whether these are faults, which were not viewed by Kisoensingh (2009) before, or the edges of a wide channel or channel belt. To give an answer to this, other stratal slices have to be analyzed.

From the cosine of instantaneous phase slice (fig. 5.3) it can be seen that the linear structure once again shows alternating values. In the middle, the structure shows values around -1, which corresponds to an instantaneous phase of  $180^\circ$  and thus a trough on a seismic wavelet. In SEG polarity that is a downward decrease in acoustic impedance. The opposite is the case at the edges of the structure and at fault locations. Here the blue colours represent zero phase, thus an downward increase in acoustic impedance. However, it is too early to predict what kind of lithology might be present. As Veeken (2007) already stated before, interpreting based on amplitudes and acoustic impedance contrasts can be highly ambiguous. For a better understanding of the structure it is better to look at the original seismic data.

In Figure 5.4 a cross section of this linear structure was taken. This cross section corresponds to inline number 1203 (the location of this is marked on figure 5.3 by white line). On this cross section, the Top of Cretaceous is shown as a pink line. In areas within the blue rectangles, the Top of the Cretaceous follows a peak, which results in a blue colour on the cosine of instantaneous phase slice. When it is following a trough (green rectangle), the cosine of instantaneous phase shows a red colour. However, this just clarifies what was stated before.

In figure 5.5, the same section of the inline is displayed, but without the Top of the Cretaceous. There it can be seen that the areas enclosed by the blue circles, might indicate the possible occurrence of a channel. However, looking at the instantaneous amplitude slice, it can be noted that these areas are characterized by low amplitudes. A possibility could be that these possible channel features are filled with clay. Referring to Van Strien (2010), this might be a possibility since Member 5 and 6 of the Upper Cretaceous consist of incised valleys. These incised valleys might have been filled with clay by a later occurring transgression. Additional evidence for an possible incised valley might come from the reflection configuration seen in figure 5.5. The reflections are discontinuous and have varying amplitudes. According to Veeken (2007), these type of reflection configurations are characterized as hummocky and they are indicative of a cut-and-fill geometry.

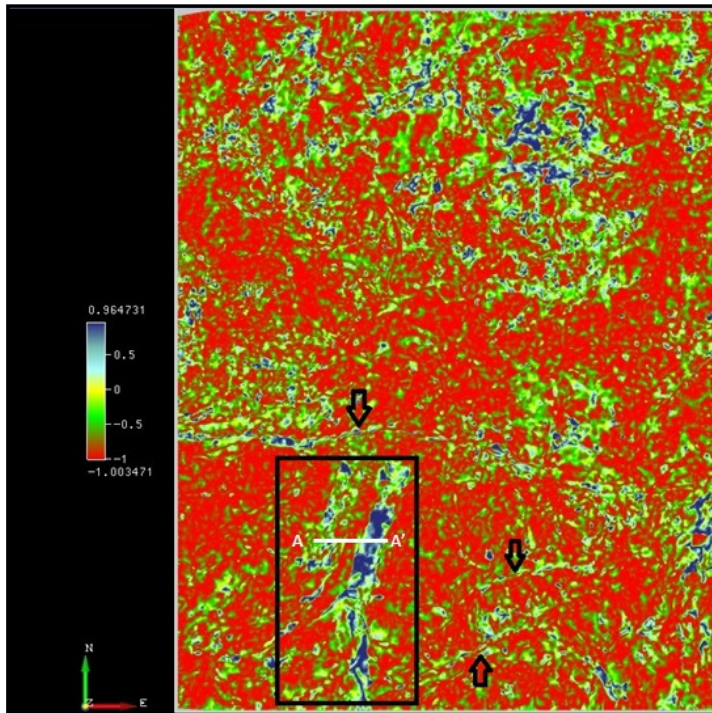


**Figure 5.3:** Cosine of instantaneous phase of the Top of Cretaceous. Top arrow indicates the EW trending fault system and bottom two arrows show the 'Broederschapsbreuk'. White line indicates cross section through the linear structure.

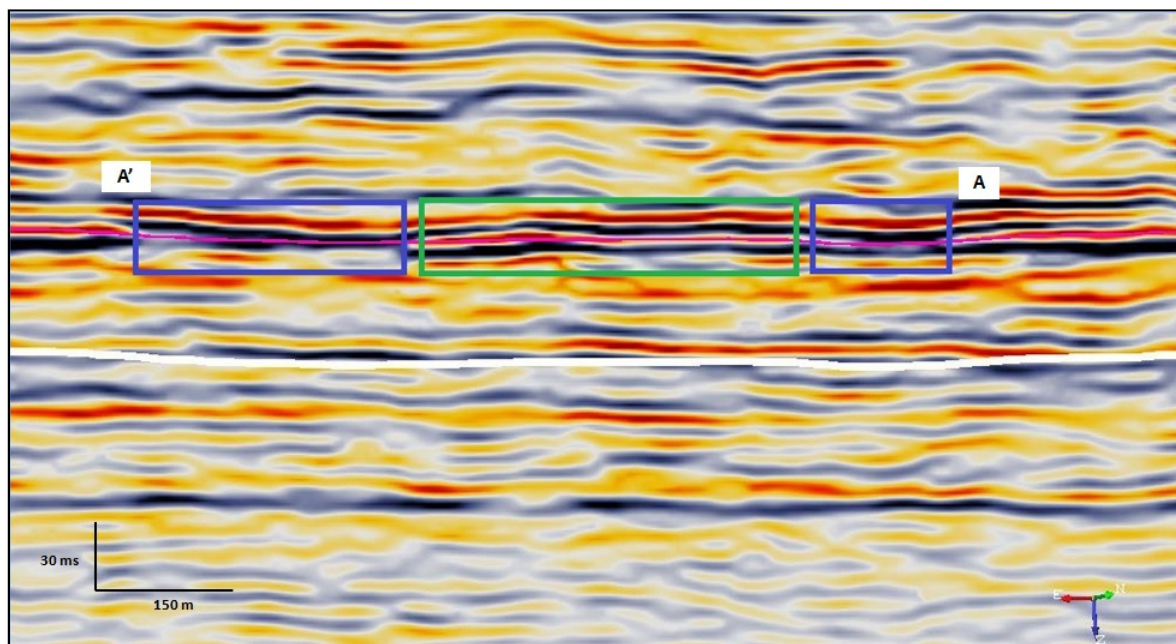


**Figure 5.4:** Image of the inline number 1203. This inline cuts through the linear structure seen in figure 5.3. The pink line represents the Top of Cretaceous and the white line the 60 ms shifted horizon.

However, Veeken (2007) also states that the amplitude is a function of the acoustic impedance contrast. The higher the velocity-density contrast, the higher the amplitude. Comparing figure 5.2, 5.3 and figure 5.6, which displays the RMS energy values at the Top of the Cretaceous, it can be noted that the middle of the linear structure has high amplitudes and an instantaneous phase of  $180^\circ$ , indicating a downward decrease in acoustic impedance. From the instantaneous frequency (figure 5.7) slice, medium to high frequencies are found in the

middle of linear structure. Note that the frequencies from the instantaneous frequency slice have extremely high values (see the colour bar in figure 5.7). These high frequency values could not yet be explained. Therefore, the frequency values are only used comparative, to locate areas with high and low frequencies. According to Taner (1992) high frequencies might be associated to shale or clay layers.

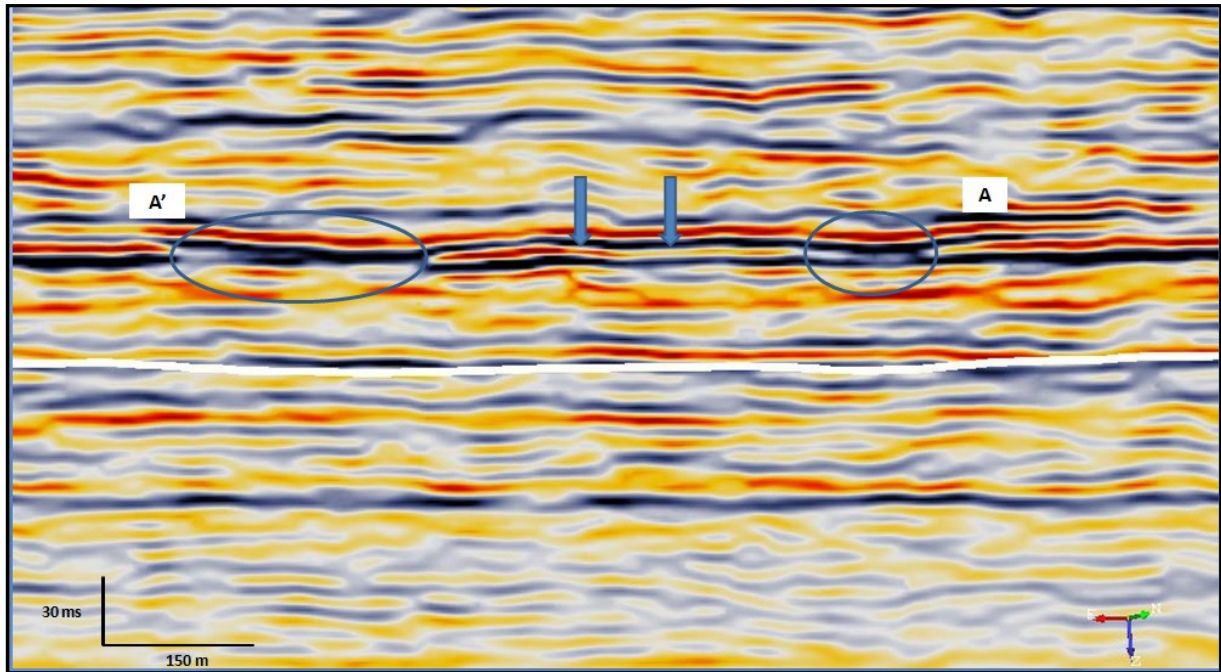


**Figure 5.5:** Image of inline number 1203. This line cuts through the linear structure seen in figure 5.3. The blue circles, enclose a possible channel feature. The area in the middle pointed out with blue arrows coincides with areas of high amplitudes.

From the high frequency values, it can be suggested that the middle of the linear structure contains clays or shales. On top of the clay or shale, there might be sands. From the high acoustic impedance contrast at the interface, it might be possible that the sands on top of the shale or clays are compacted, which increases their acoustic impedance contrast at the interface and results in high amplitudes at that location.

From figure 5.1, 5.3, 5.6 and figure 5.7, it can be noted that the edges of the linear structure, which were described as possible channel features in figure 5.5, have low amplitudes, relatively lower frequencies and show a downward increase in acoustic impedance. From what Taner (1992) stated, it is possible that these channel features contain sand. But possibly due to their fluid content, they have lower velocity- density contrasts with above lying lithologies, and therefore show lower amplitudes. Further it can be seen that the thin bed indicator slice (figure 5.8) shows some anomalies along the edges of this structure. These

frequency anomalies at the edges might indicate thinning of sands towards the edges, which causes interference of reflectors and thus distortions in the frequency.

So from the above we can conclude that the linear structure found in the south is possibly a channel belt, which transported clastic material, most likely sands, from the Proterzoic basement northwards. These channels are probably thick in the middle and thin towards the edges.

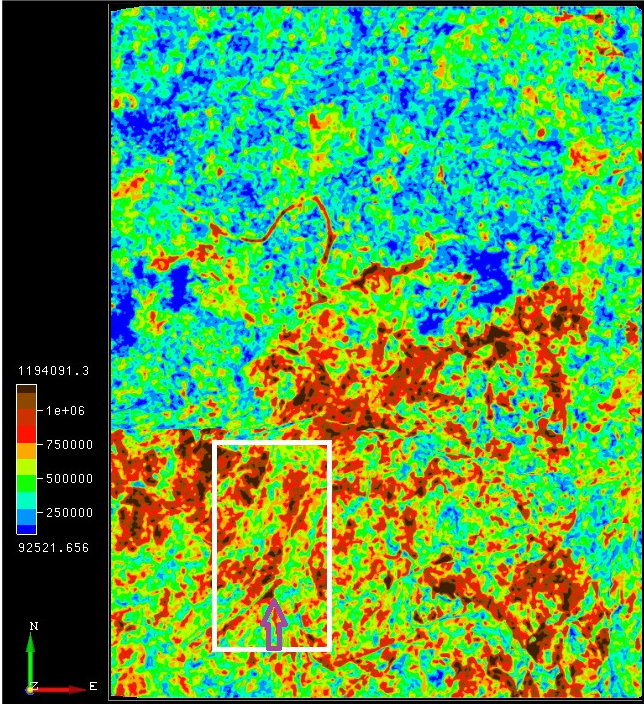


**Figure 5.6:** RMS energy slice of the Top of Cretaceous. The purple arrow indicates high RMS energy, related to high amplitudes, in the middle of the linear structure (within the white box).

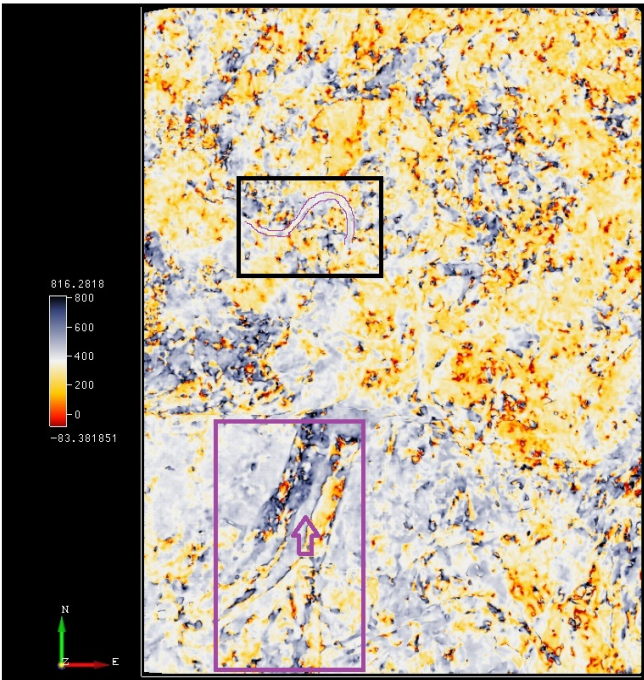


**Figure 5.7:** Instantaneous frequency slice of the Top of Cretaceous. Northern channel feature has been edited to visually enhance the image. The edges of the channel have been coloured purple. The middle of the linear structure (purple box) is indicated by a purple arrow.

Coming back to the northern channel feature displayed in figure 5.1 and 5.2, this channel shows middle to high frequencies on the frequency slice in figure 5.7. These relative high frequencies might indicate a thin shale (or clay) or sand bed below vertical resolution. However, on the thin bed indicator slice, the channel feature has constant values. As Taner (1992) stated before, such a smooth variation in the thin bed indicator values are still inexplicable. Similarly to middle the channel belt structure in the south, this channel is displayed with high amplitudes (figure 5.1), low cosine of instantaneous phase (figure 5.3) and high frequencies (figure 5.7). It might thus also be possible, that this is similar to the middle of the possible channel belt, a clay or shale deposit. If this channel is filled by clay or shale, it is thus possible that due to a later transgression, clay was deposited there. This channel lies more seawards (northwards) so it is likely that a transgression might have filled this channel with clayey deposits.

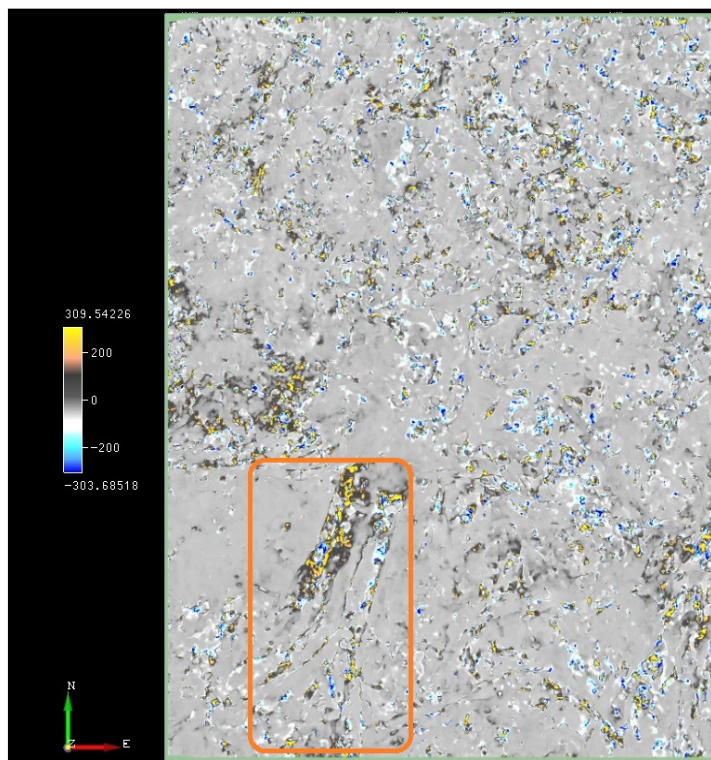


**Figure 5.8:** Thin bed indicator slice of the Top of Cretaceous. Orange box delineates the southern channel feature with anomalies in thin bed indicator.

During the attribute analysis the RMS energy, instantaneous phase and instantaneous phase have been blended together in a RGB display. The RMS energy was plotted against red, instantaneous phase against green and instantaneous frequency against blue colours. As a result the blending gave a better delineation of the channel features as can be seen in figure 5.9.

Interpreting the similarity stratal slice below the Top of Cretaceous (figure 5.10), it can be seen that the interpreted southern channel is not any more visible on the stratal slice. On this slice, only a part of the northern channel feature (highlighted in red) is visible and also another channel (highlighted by orange) with an SE-NW trend (figure 5.10). This slice also revealed all the faults interpreted on the Top of Cretaceous. However the cosine of the instantaneous phase (figure 5.11) slice still shows a certain structure in the southern part was the southern channel feature was depicted. This structure shows values of minus one for the cosine of instantaneous phase, indicating that there should be a downward decrease of acoustic impedance. From the RMS energy slice (figure 5.12) relatively low amplitudes are found in that area. It might be thus possible, that there are either clay or shales present now.

High amplitudes are now found in the south-eastern section of the slice (figure 5.12). These high amplitudes coincide with cosine of instantaneous values of one, thus indicating a downward increase in acoustic impedance. From the instantaneous frequency slice (figure 5.13), it is noticeable that this section also corresponds to low frequencies. From what is seen on the slices it might thus possible that this area corresponds to sand deposits.

Further it can be seen that the section containing high amplitudes, is bordered by a NNW-SSE trending fault and the ENE-WSW trending 'Broederschapsbreuk' (figure 5.12). The NNW-SSE fault is not mentioned by Kisoensingh (2009). It might be possible that this a NS trending fault mentioned before by Kisoensingh (2009). From the instantaneous frequency slice (figure 5.13) these fault areas are marked by a lot of frequency anomalies. If this section contains indeed sand deposits, it might be possible that due to thinning out at fault locations, the fault locations show frequency anomalies.

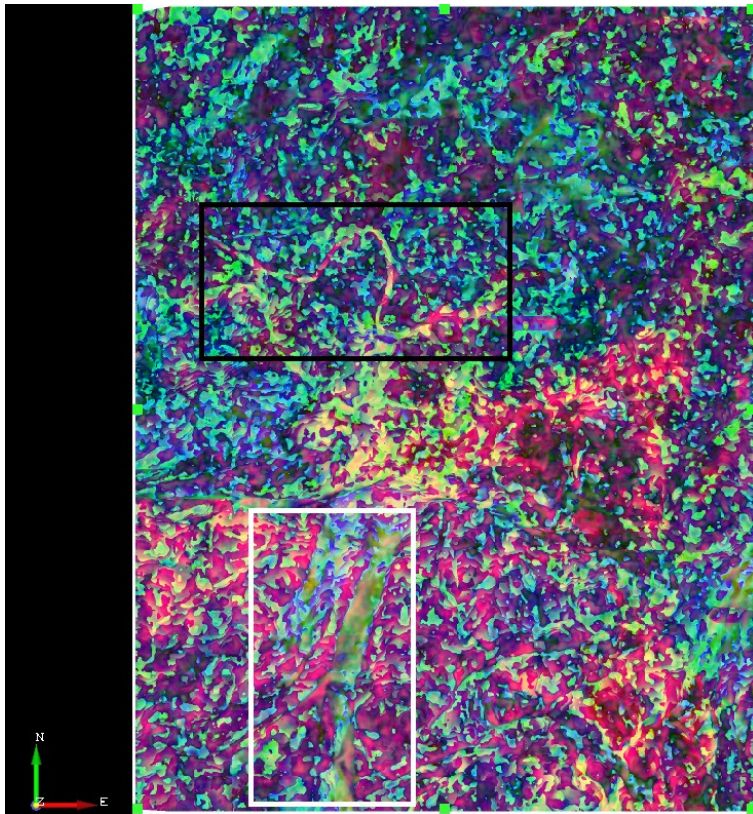


**Figure 5.9:** RGB blend of RMS energy (red colour), instantaneous phase (green) and instantaneous frequency (blue).

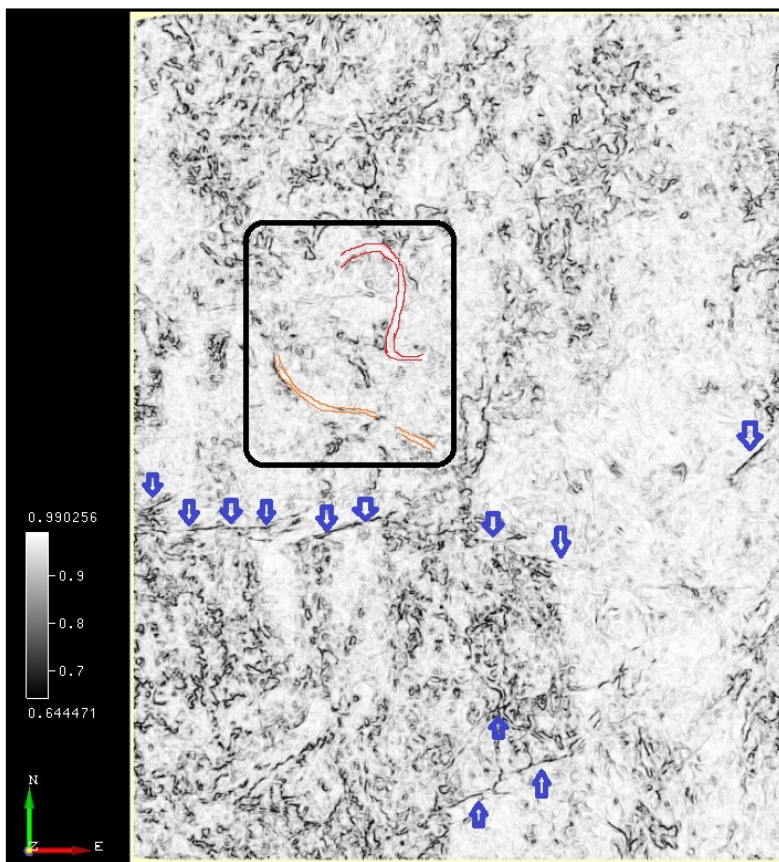


**Figure 5.10:** Similarity stratal slice below the Top of Cretaceous. Faults are indicated by blue arrows. In the black rectangular two channels can be seen. The edges of these channels are highlighted by red and orange colours.

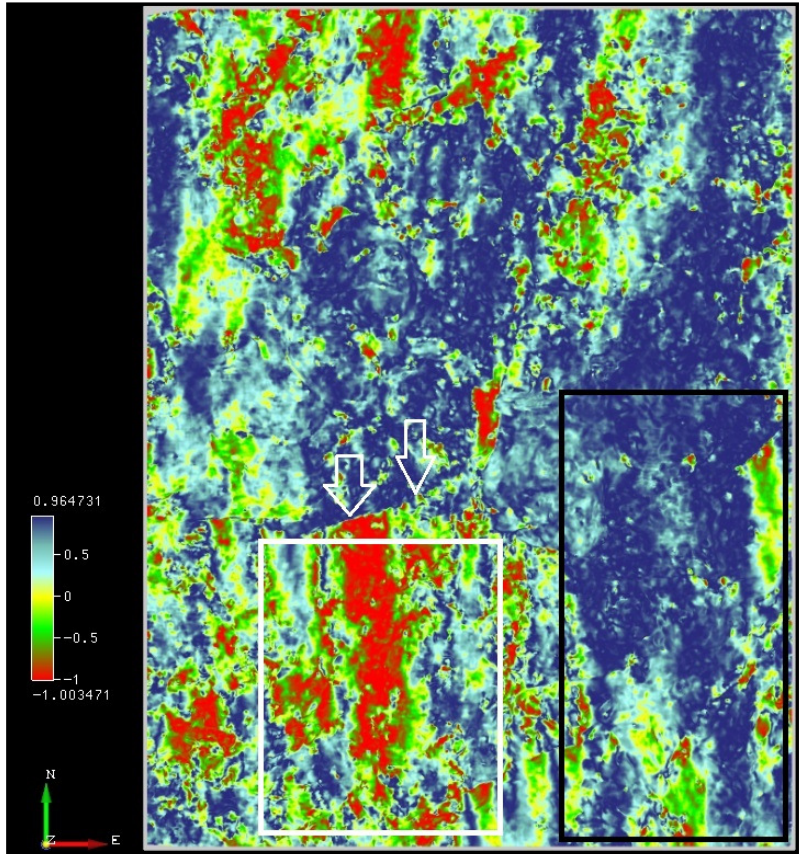


**Figure 5.11:** Cosine of the instantaneous phase stratal slice below the Top of the Cretaceous. White rectangle shows the area where the linear structure was found at the Top of the Cretaceous. Black rectangle delineates area where high amplitudes can be found in figure 5.12.

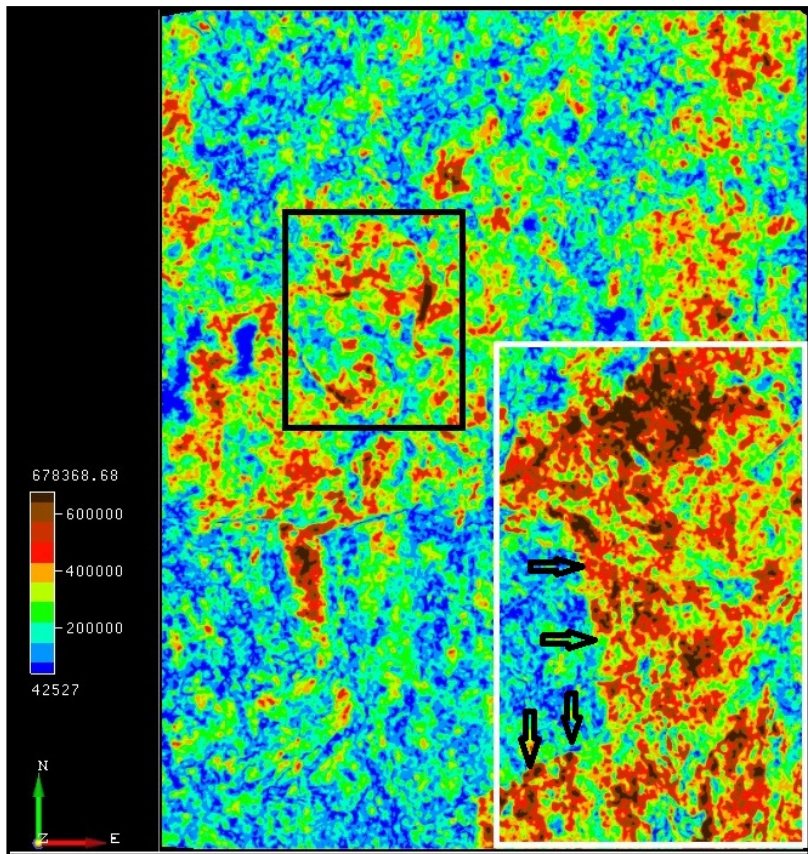


**Figure 5.12:** RMS energy stratal slice below the Top of the Cretaceous. Black rectangle highlights the area where most likely the channel features occur, showing high amplitudes. The white rectangle highlights section of high amplitudes in the southeastern part of the study area. The black arrows indicate faults. The horizontal arrows indicate the NNW-SSE fault and the vertical arrows indicate the 'Broederschapsbreuk'.

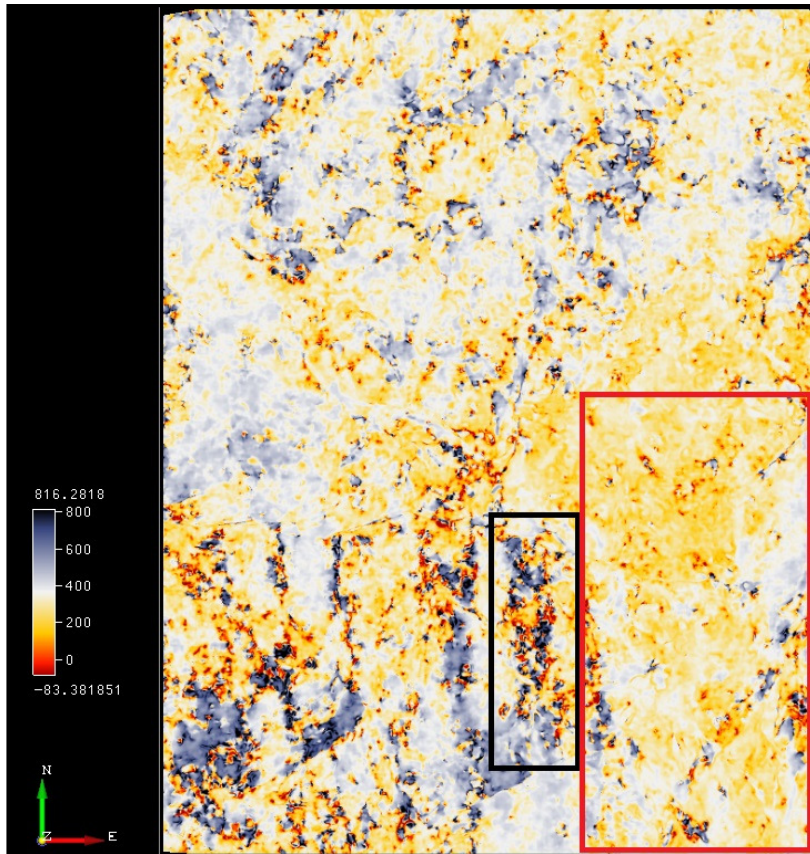


**Figure 5.13:** Instantaneous frequency stratal slice below the Top of the Cretaceous. Red rectangle marks area with high amplitudes. Black rectangles marks frequency anomalies at NNW – SSE fault location.

This pattern of high amplitudes in the south-eastern section holds on till the second and third slice under the Top of Cretaceous and thereafter there is an irregular pattern of amplitudes visible in the whole area (Appendix B). The instantaneous frequency remains to have the same in pattern from the first to third stratal slice below the Top of Cretaceous. However, the cosine of instantaneous phase changes, completely from the second stratal slice onwards (figure 5.14). It is thus possible that there is more or less a uniform lithology present from the second slice onwards. But what this lithology is, cannot be predicted.

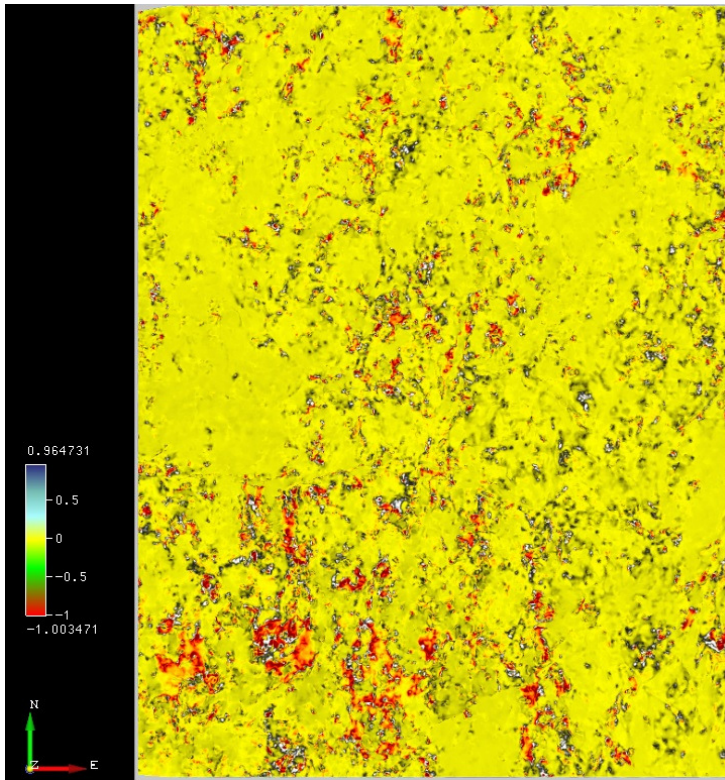


**Figure 5.14:** Cosine of instantaneous phase. This is the pattern from the second stratal slice below the Top of Cretaceous and onwards.

### *Geologic history construction*

From this attribute analysis it can be concluded that during the Upper Cretaceous there were some active channels, most likely flowing from the South to the North and feeding the basin with erosional products such as sands from the Proterozoic basement. The channel feature found on the southern side of the EW trending faults was most likely the feeder channel of the other channels more northwards from this fault. As mentioned by Kisoensingh (2009), the EW trending fault was a strike slip fault, which displaced vertically at the end of the Cretaceous. Although the stratal slices corresponded to one point in geological time, it might be possible that the part south of the EW trending fault was uplifted due to normal faulting, which made the channel indistinguishable in the stratal slices below the Top of the Cretaceous. Further it can be also stated that faulting was active during the Cretaceous. The NNW- SSE fault trend for example was visible in lower stratal slices and not at the Top of the Cretaceous stratal slice.

### ***Lithology or Lithofacies prediction***

Although not all stratal slices have been analyzed by the unsupervised neural network, the UVQ segmentation at the top of the Cretaceous might give a prediction of the distribution of different lithologies or lithofacies at this horizon. Figure 5.15 shows the result of the segmentation. In the UVQ segmentation the number of classes was set at five. This is distinguishable as five different colours (yellow, red, blue, white/gray and black) on the image. From this image, the channel feature in the north and the possible channel belt in the south, interpreted as a linear structure before, are clearly distinguishable. As what was predicted before, the middle of the channel belt structure and northern channel feature might consist of the same lithology. The UVQ segmentation can thus be used to quality control lithology predictions. The red and black colours might indicate sands as what was predicted before, but for the other classes (other colours) no prediction can be made. However, it is not known if the previous predictions are correct or not. These findings still have to be validated and calibrated with well data to give an adequate prediction.

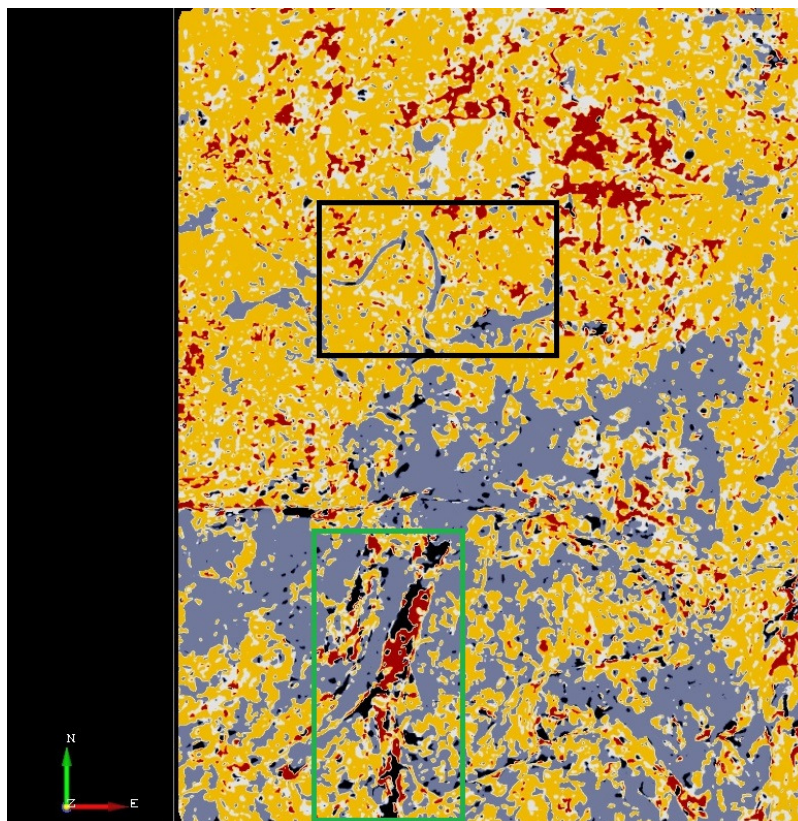


**Figure 5.15:** UVQ using the instantaneous frequency, RMS energy and cosine of instantaneous attribute. The UVQ is run along the Top of the Cretaceous. Black rectangle depicts possibly channel feature containing sand. Green rectangle shows a possible belt.

## **6 Conclusion and Recommendations**

### **6.1 Conclusion**

The main objective of this study was to conduct a deterministic and qualitative seismic attribute analysis for the purpose of delineating geological features of interest as well as finding and predicting the distribution of lithofacies in the uppermost Cretaceous below the Tambaredjo field in Suriname. After a literature research, the following attributes were selected and used for this analysis: instantaneous frequency, instantaneous amplitude, cosine of instantaneous phase, RMS energy, thin bed indicator, instantaneous Q factor, variance, similarity and spectral decomposition. However, after analyzing the data, it was found that not all the attributes were useful for reaching the objective. The most effective attributes were instantaneous frequency, cosine of instantaneous phase, instantaneous amplitude, similarity and RMS energy. The other attributes furnished less or no contribution to the interpretation.

The interpretation resulted in the identification of several structural and stratigraphic features such as channels and faults. Also a raw estimation was made of the distribution of lithofacies in the Upper Cretaceous. These results also provide a better understanding of the geology of the Upper Cretaceous. Nonetheless, this interpretation is for a large part preliminary as the findings still have to be validated and calibrated with well data. Furthermore, the interpreter's bias might have caused errors during the attribute calculations, which may have affected the findings of this study.

## 6.2 Recommendations

Although some of the attributes have been effective in delineating stratigraphic and structural features and also helped in creating a better understanding of the possible distribution of some lithologies or lithofacies, there are still some suggestions which might improve the attribute analysis.

First of all, based on some problems that have occurred during this study, the following things should be taken under consideration:

- The polarity of seismic data has always to be checked
- The interpretation of the Top of Cretaceous has to be improved (preferably manually) and it should be calibrated by well data in order to locate its true position

Concerning the attributes used, some suggestions are:

- The instantaneous Q factor should probably be used in vertical time slices instead of stratal slices. According to Pigott et al. (2013) this attribute has been proven effective in vertical time slices.
- The thin bed indicator should further be investigated. Although, it was able to give an indication at possible channel edges and at fault locations, this attribute could not give more information at the northern channel feature. Another option would be to use the thin bed indicator proposed by Sun et al. (2010).
- The frequency values in the instantaneous frequency attribute need to be checked. This is also the case for all the values in an attribute analysis. These immensely high values were most likely the reason for the ineffective spectral decomposition attribute, which was highly recommended by several authors.
- The similarity attribute on its own is effective in delineating faults.

Further, Schram de Jong (2003) was able to detect Paleocene reservoir sands using supervised neural networks. It is thus highly suggested to use supervised neural networks for detecting sands (which could be possible reservoirs) in the Cretaceous interval.

## References

- Barnes, A. E. (1993). Instantaneous spectral bandwidth and dominant frequency with applications to seismic reflection data. *Geophysics*, 58(3), 419–428.
- Brown, A. R. (2004). *Interpretation of Three-Dimensional Seismic Data* (6th ed.). Tulsa, Oklahoma: The American Association of Petroleum Geologist and the Society of Exploration Geophysicist.
- Chehrazi, a., Rahimpour-Bonab, H., & Rezaee, M. R. (2013). Seismic data conditioning and neural network-based attribute selection for enhanced fault detection. *Petroleum Geoscience*, 19(2), 169–183. doi:10.1144/petgeo2011-001
- Chopra, S., & Marfurt, K. J. (2005). Seismic attributes — A historical perspective. *Geophysics*, 70(5), 3SO– 28SO. doi:10.1190/1.2098670
- Chopra, S., & Marfurt, K. J. (2007). *Seismic Attributes for Prospect Identification and Reservoir Characterization*. Tulsa, United States of America: Society of Exploration Geophysicists.
- Chopra, S., & Marfurt, K. J. (2008). Emerging and future trends in seismic attributes. *The Leading Edge*, 27(3), 298–318. doi:10.1190/1.2896620
- De Rooij, M., & Tingdahl, K. (2002). Meta-attributes—the key to multivolume, multiattribute interpretation. *The Leading Edge*, 21(10), 1050–1053. doi:10.1190/1.1518445
- Galloway, W. E., & Hobday, D. K. (1996). Terrigenous clastic depositional systems. Application to fossil fuel and groundwater resources. *Sedimentary Geology* (2nd ed., Vol. 112). Springer-Verlag Berlin Heidelberg New York. doi:10.1016/S0037-0738(97)00032-8
- Halliburton. (2013). Instantaneous phase. Retrieved from [http://esd.halliburton.com/support/LSM/DSD/DSD/5000/5000\\_8/Help/mergedProjects/attributes/instant\\_phase.htm](http://esd.halliburton.com/support/LSM/DSD/DSD/5000/5000_8/Help/mergedProjects/attributes/instant_phase.htm)
- Hesthammer, J., Landrù, M., & Fossen, H. (2001). Use and abuse of seismic data in reservoir characterisation. *Marine and Petroleum Geology*, 18(5), 635–655. Retrieved from <http://linkinghub.elsevier.com/retrieve/pii/S0264817201000113>
- Kisoensingh, S. D. (2009). Evolution and timing of fault systems relative to sedimentation and trapping in the Tambaredjo Field area , Suriname Application of the resulting “ geo □ structural ” model outside the Tambaredjo 3D seismic area. University of Utrecht.
- Kuroda, M. C., Vidal, A. C., & de Carvalho, A. M. A. (2012). Interpretation of seismic multiattributes using a neural network. *Journal of Applied Geophysics*, 85, 15–24. doi:10.1016/j.jappgeo.2012.06.009
- Liu, J., & Marfurt, K. J. (2007). Instantaneous spectral attributes to detect channels, 72(2).

- Nandlal, B., & Mwakipesile-Arnou, L. (1998). *Geology of the Tambaredjo Reservoir*.
- Pigott, J. D., Kang, M.-H., & Han, H.-C. (2013). First order seismic attributes for clastic seismic facies interpretation: Examples from the East China Sea. *Journal of Asian Earth Sciences*, 66, 34–54. doi:10.1016/j.jseaes.2012.11.043
- Potter, P. E. (1997). The Mesozoic and Cenozoic paleodrainage of South America: a natural history. *Journal of South American Earth Sciences*, 10(5-6), 331–344. doi:10.1016/S0895-9811(97)00031-X
- Qayyum, F., de Groot, P., & Heemstra, N. (2012). Using 3D Wheeler diagrams in seismic interpretation- the HorizonCube method. *First Break*, 30, 103 – 109.
- Rabelo, I. R. (2006). 3D Geological Object Recognition in High-Resolution Seismic Data. A Case Study from a Palaeocene Fluvio-Estuarine Reservoir in Suriname. Delft University of Technology.
- Raeesi, M., Moradzadeh, A., Doulati Ardejani, F., & Rahimi, M. (2012). Classification and identification of hydrocarbon reservoir lithofacies and their heterogeneity using seismic attributes, logs data and artificial neural networks. *Journal of Petroleum Science and Engineering*, 82-83, 151–165. doi:10.1016/j.petrol.2012.01.012
- Rezvandehy, M., Aghababaei, H., & Raissi, S. H. T. (2011). Integrating seismic attributes in the accurate modeling of geological structures and determining the storage of the gas reservoir in Gorgan Plain (North of Iran). *Journal of Applied Geophysics*, 73(3), 187–195. doi:10.1016/j.jappgeo.2010.12.008
- Schram de Jong, A. C. (2003). Detection of the T sands in the Tambaredjo Oil Field, Suriname, by application of an artificial neural network to 3D seismic data. Delft University of Technology.
- Shi, W., Zhao, Z., Jiang, T., Miao, H., & Wang, X. (2012). Identifying updip pinch-out sandstone in nearshore subaqueous fans using acoustic impedance and the instantaneous phase in the Liangjia area, Yitong Basin, China. *Marine and Petroleum Geology*, 30(1), 32–42. doi:10.1016/j.marpetgeo.2011.10.010
- Subrahmanyam, D., & Rao, P. H. (2008). *Seismic Attributes- A Review*. Hyderabad.
- Sun, L.-P., Zheng, X.-D., Shou, H., Li, J.-S., & Li, Y.-D. (2010). Quantitative prediction of channel sand bodies based on seismic peak attributes in the frequency domain and its application. *Applied Geophysics*, 7(1), 10–17. doi:10.1007/s11770-010-0009-y
- Taner, M. . T. (2001). Seismic Attributes. *CSEG Recorder*, 26(7), 49 – 56.
- Taner, T. M. (1992). ATTRIBUTES REVISITED. *Attributes Revisited*. Retrieved July 15, 2013, from [http://rocksolidimages.com/pdf/attrib\\_revisited.htm#\\_Toc328470864](http://rocksolidimages.com/pdf/attrib_revisited.htm#_Toc328470864)
- Veeken, P. C. H. (2007). Seismic Stratigraphy, Basin Analysis and Reservoir Characterisation. (K. Helbig & S. Treitel, Eds.) (Handbook o.). Amsterdam, The Netherlands: Elsevier B.V.

- Wong, T. E. (1989). Revision of the Stratigraphy of the Coastal plain of Suriname (p. 64). Foundation for Scientific Research in the Caribbean.
- Workman, W., & Birnie, D. J. (2007). The Guyana-Suriname Basin : An Evolving Exploration Opportunity. *Let it flow CSPG CSEG Convention*, 289–292.
- Xia, S., Liu, J., Deng, J., Li, P., Ren, Y., Chang, Y., Liu, J. (2013). River channel sand body prediction by means of integrating well log and seismic attribute analysis in dense well patterns: a case study of the eastern Beiherxi Block in the Sabei Development Area of Daqing Oilfield, China. *Arabian Journal of Geosciences*. doi:10.1007/s12517-013-0833-5
- Zhang, J.-H., Liu, Z., Zhu, B.-H., Feng, D.-Y., Zhang, M.-Z., & Zhang, X.-F. (2011). Fluvial reservoir characterization and identification: A case study from Laohekou Oilfield. *Applied Geophysics*, 8(3), 181–188. doi:10.1007/s11770-011-0288-y
- Zhang, Q., Member, S., & Gupta, K. C. (2003). Artificial Neural Networks for RF and Microwave Design — From Theory to Practice. *IEEE Transactions on Microwave Theory and Techniques*, 51(4), 1339–1350. doi:0018-9480/03
- Other documents:*
- Halliburton. (2009). Conceptual Geological and Depositional Model - Tambaredjo NW Field , Suriname.
- POC Team. (2008). *Prospectivity Evaluation and Work program proposal of the Near shore Blocks 3 and 4*. Paramaribo, Suriname.
- RET. (2012). Tambaredjo 3D Cretaceous Exploration Program 2012. Paramaribo, Suriname.
- Van Strien, W. J. (2010). SEQUENCE STRATIGRAPHY OF THE CRETACEOUS NICKERIE FORMATION , ONSHORE SURINAME : IMPLICATIONS FOR HYDROCARBON. Internal report Staatsolie Maatschappij Suriname N.V. Paramaribo, Suriname.
- Diephuis, G. (2012). Lecture slides course Geologic interpretation of seismic data, Delft University of Technology.

---

## **Appendices**

---

## Appendix A      Seismic wavelet, polarity and resolution

### Seismic wavelet

Before concepts of seismic polarity and resolution can be described, we have to get an understating of a seismic wavelet. A seismic wavelet is the convolution of earth's response with a time series representation of the source signal. The key attributes of a wavelet are amplitude, frequency and phase. Figure A.1 describes the main terminologies used in seismic wavelets.

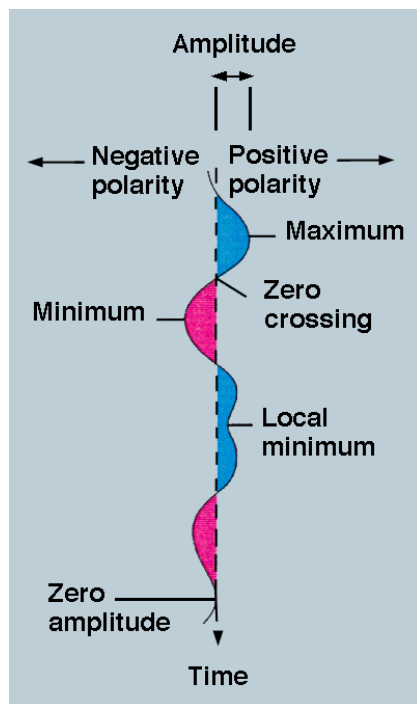


Figure A.1: Terminology used for seismic wavelets (Haverkamp, 2002)

There are different wavelet shapes, but the two most used wavelet shapes are the zero phase and minimum phase (figure A.2). In a minimum-phase wavelet the start of the wavelet coincides with the exact position of the subsurface interface, whereas in a zero-phase wavelet, the maximum amplitude of the wavelet coincides with the subsurface interface. A zero-phase wavelet is symmetric around the seismic event that caused it. In seismic data processing a zero-phase wavelet is preferred, because it can be used to locate acoustic impedance interfaces (Veeken, 2007).

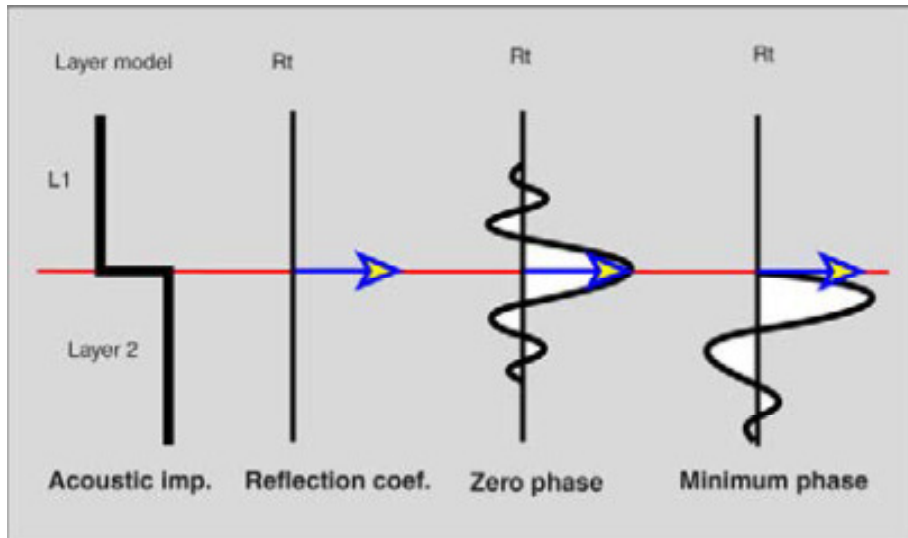


Figure A.2: The minimum phase and zero phase wavelets. In this image it is clearly shown that the interface with acoustic impedance contrast coincides with the maximum amplitude of a zero phase wavelet and the start position of a minimum phase wavelet (Veeken, 2007).

### Seismic polarity

Polarity relates to the way how a seismic trace is drawn on a seismic section as a result of acoustic impedance contrasts. There are two conventions used in seismic data, the SEG (Society of Exploration Geophysicist) polarity which is mostly used in the United States of America and the Non-SEG polarity or European polarity. According to Veeken (2007) the polarity is important in determining lithology changes. The polarity is thus also crucial in for example a seismic well tie. A downward increase in acoustic impedance (hard kick) has by SEG convention a positive polarity and it is displayed as a blue peak on a density display (figure A.3). A downward decrease in acoustic impedance, however has by SEG convention a negative polarity and is displayed as a red trough on the density display (figure A.4).

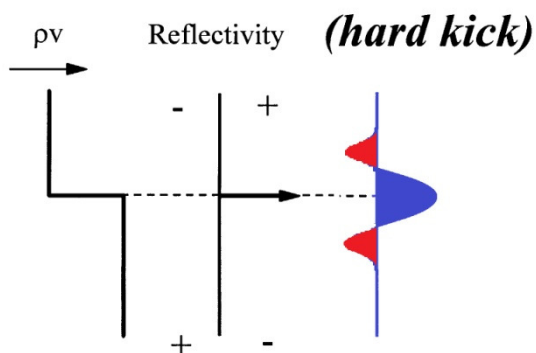


Figure A.3: Density display of zero-phase wavelet in SEG positive polarity (modified from lecture notes Diephuis, 2012)

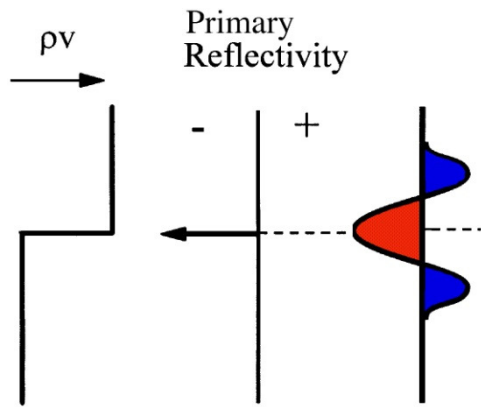


Figure A.4: Density display of zero-phase wavelet in SEG negative polarity (modified from lecture notes Diephuis, 2012)

### Tuning effects, vertical and horizontal resolution

The tuning effect can be defined as the interference of wavelets from vertically closely spaced reflectors. If two reflectors have a small vertical distance, their two-way-travel time interval becomes smaller, which results in overlapping of their wavelets. This overlapping will create a composite complex waveform (Veeken, 2007). However, interference can be constructive and destructive. In a constructive interference, the waveform's amplitude is magnified. The opposite is the case in destructive interference (figure A.5).

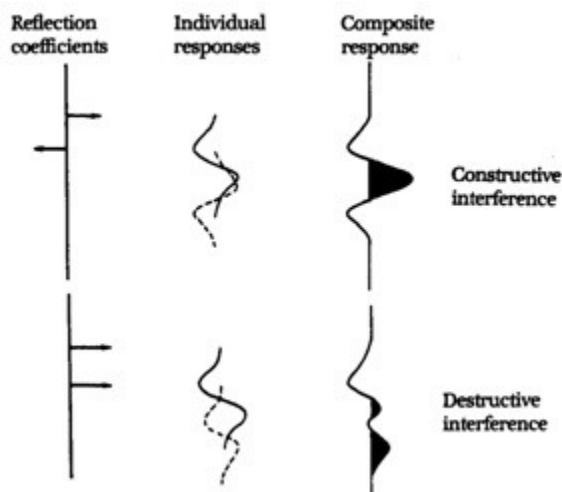


Figure A.5: Example of constructive and destructive interference for a minimum-phase wavelet (Haverkamp, 2002)

On seismic sections, usually layers with a minimum thickness of  $\frac{1}{4} \lambda$  can be imaged. This thickness is called the tuning thickness or the bed-thickness resolution (Veeken, 2007). The bed-thickness resolution or vertical resolution, decreases with increasing depth. This is

because of the absorption of higher frequencies with depth. Further a bad signal-to-noise ratio (S/N) can also decrease the vertical resolution. However, stacking might decrease the signal-to-noise ratio.

Apart from vertical resolution limitation, horizontal resolution limitation also exist. The horizontal resolution depends on the distance between subsurface sampling points. An important concept in horizontal resolution is the Fresnel zone. When a geophone or hydrophone receives a signal, this signal does not only contain the reflection energy of one single subsurface point, but it includes also energy from neighbouring points. The circular area containing to the energy of the reflected signal, is the Fresnel zone. To improve the horizontal resolution, the width of the Fresnel zone has to be decreased. This can be done during migration. The Fresnel zone can be given by the following relation:

$$rf = \frac{V}{2} \sqrt{\frac{t}{F}}$$

where :

rf = radius of Fresnel zone (m)

V = average velocity (m/s)

t = two - way - time (s)

F = dominant frequency (Hz)

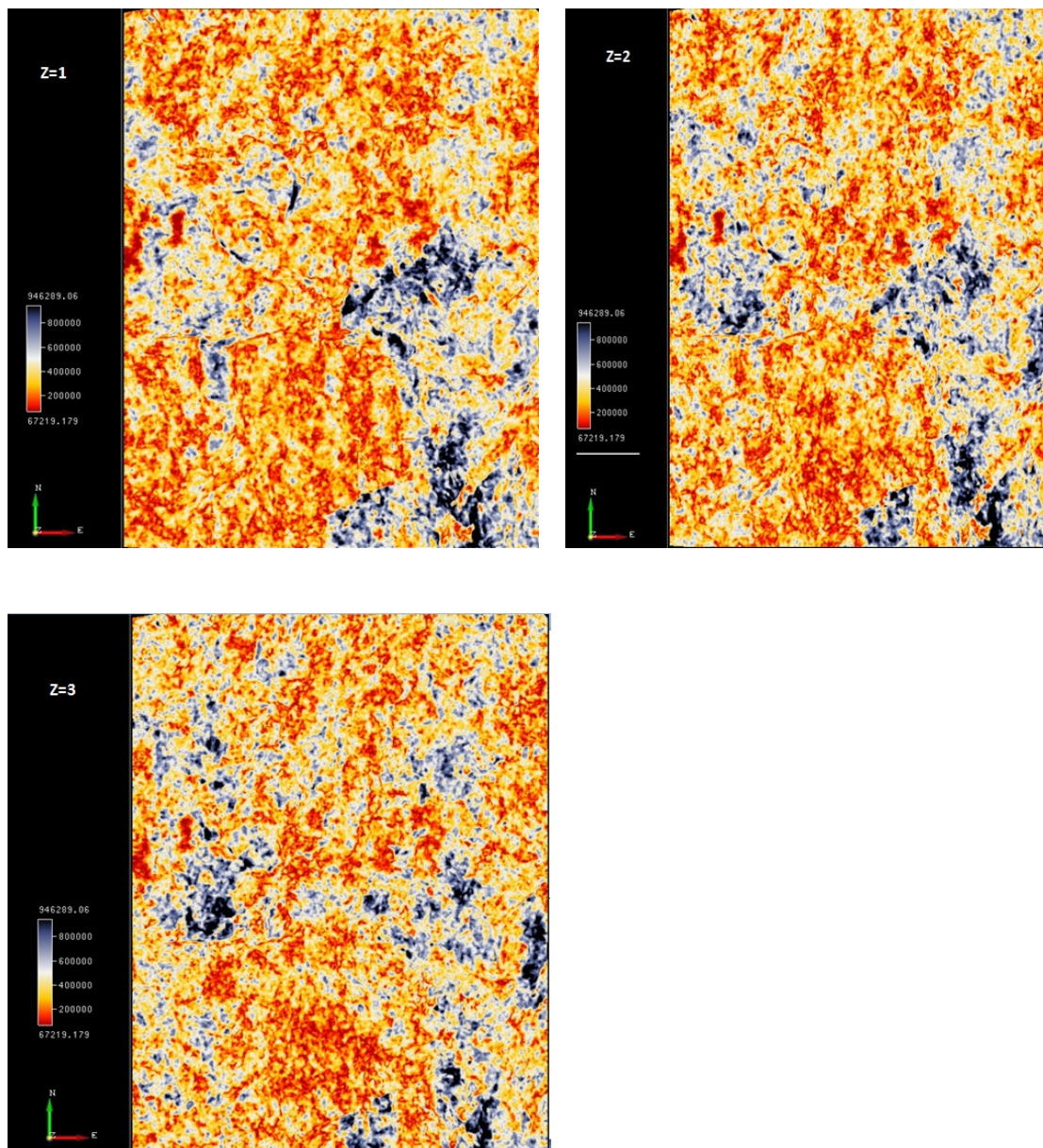
## Appendix B      Seismic Attribute Maps

This appendix contains the attribute maps which were generated but not viewed in chapter 5.

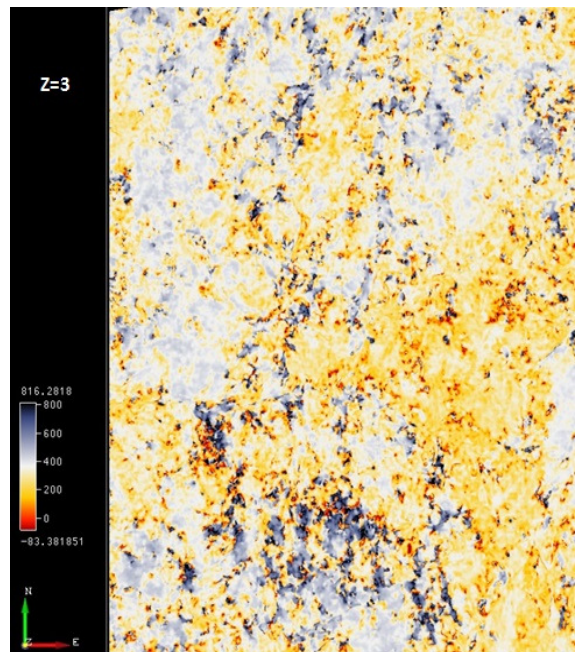
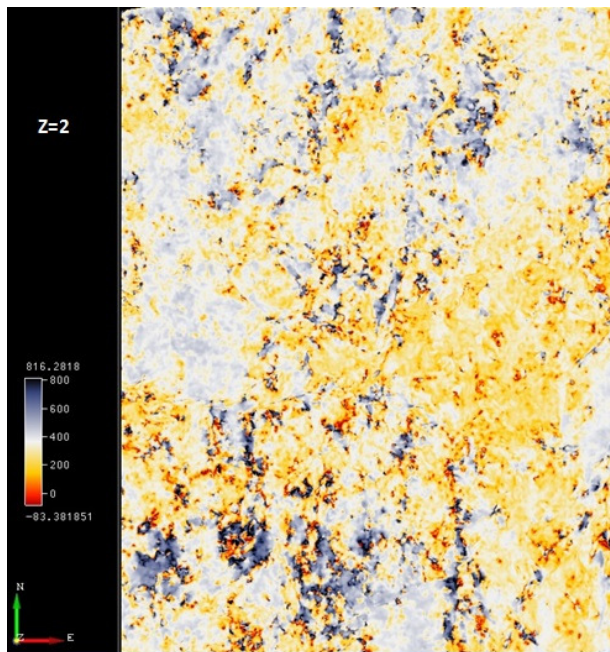
Please note the terminology:

- Z=0 → Top of Cretaceous stratal slice
- Z=1 → stratal slice below Top of Cretaceous
- Z=2 → second stratal slice below Top of Cretaceous
- Z=3 → third stratal slice below Top of Cretaceous

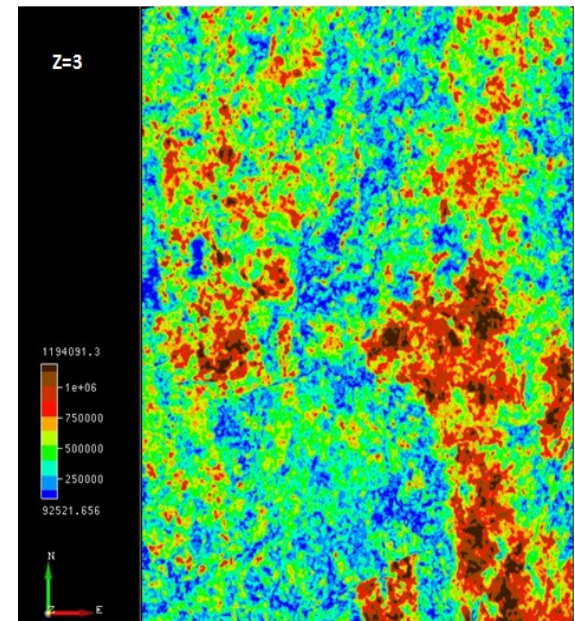
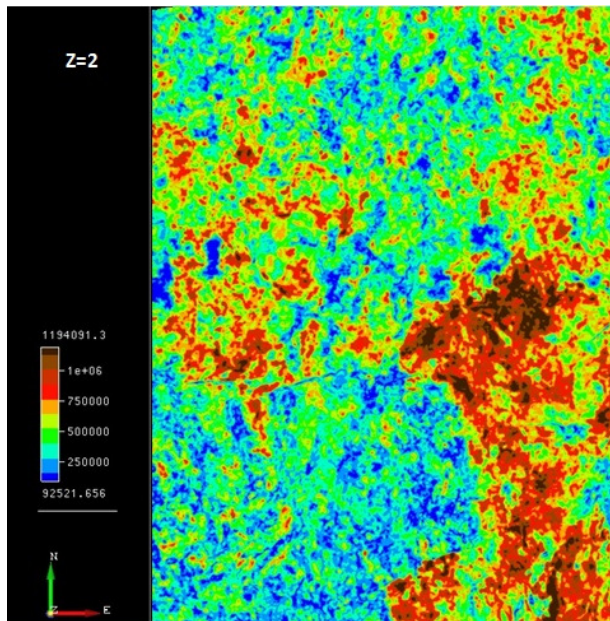
### *Instantaneous Amplitude*



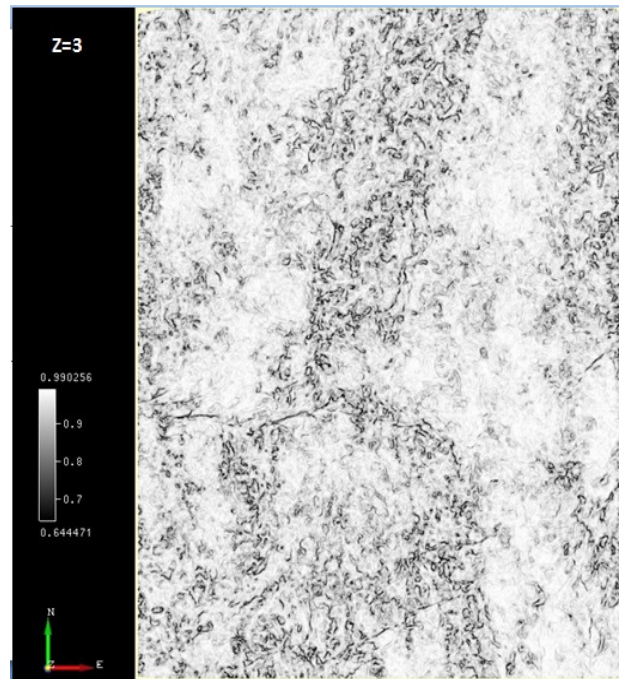
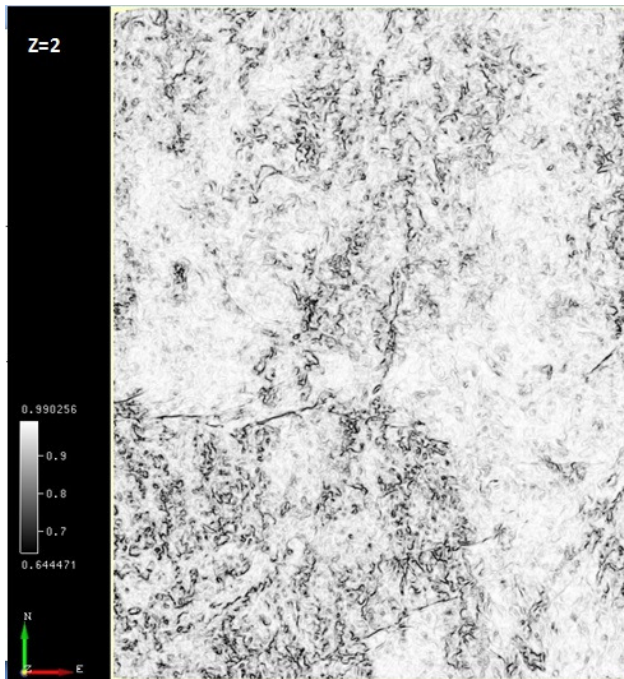
*Instantaneous frequency*



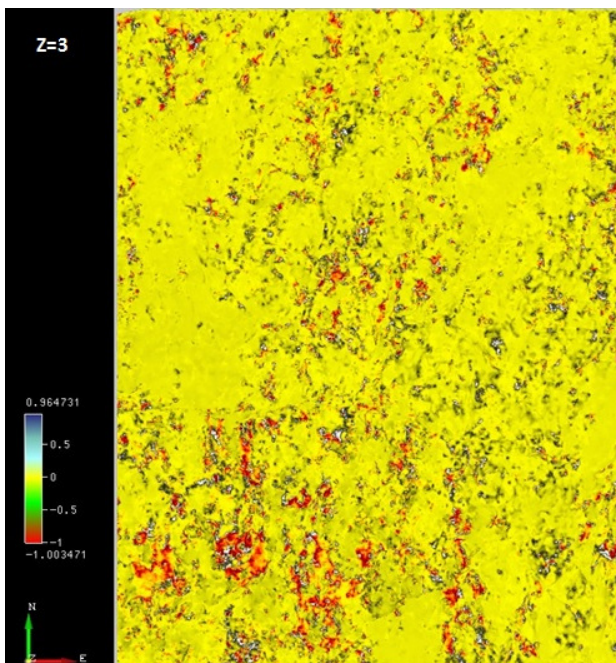
*RMS energy*



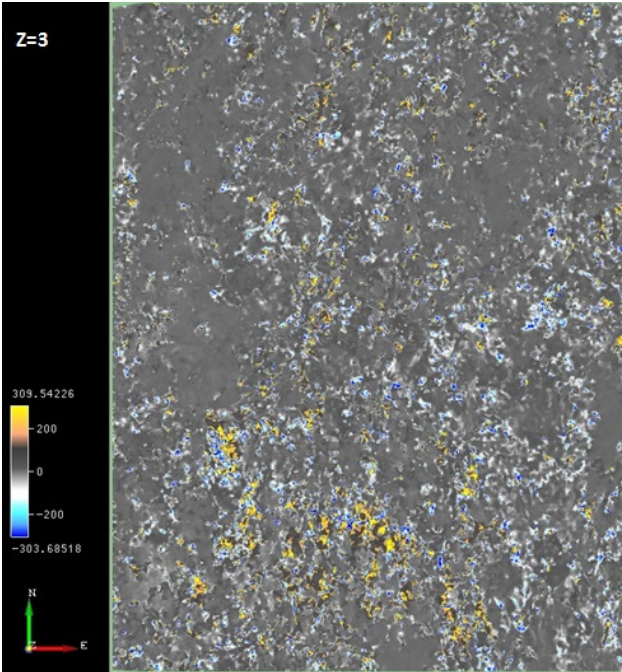
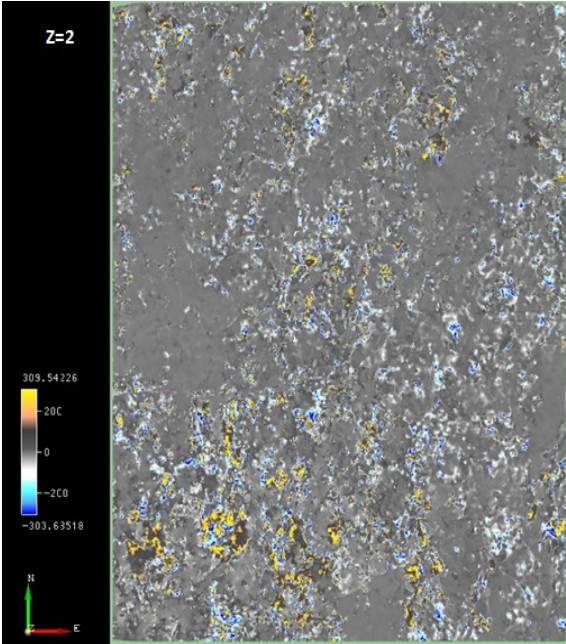
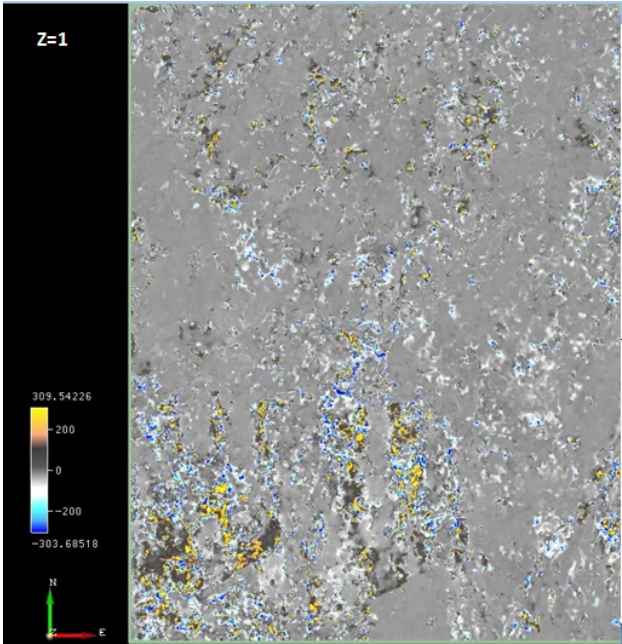
*Similarity*



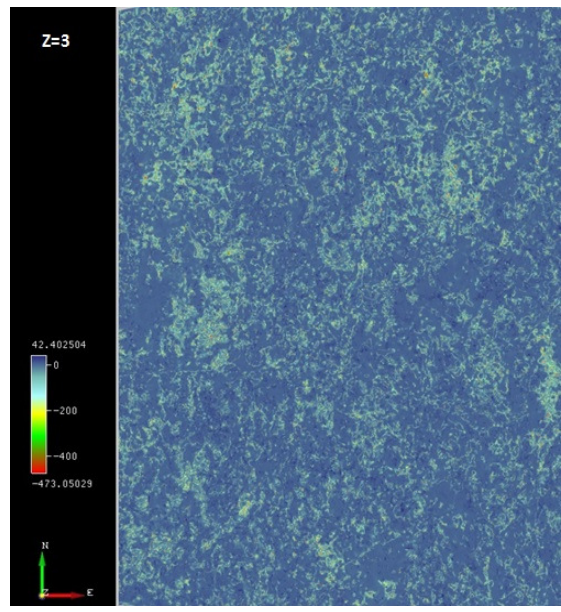
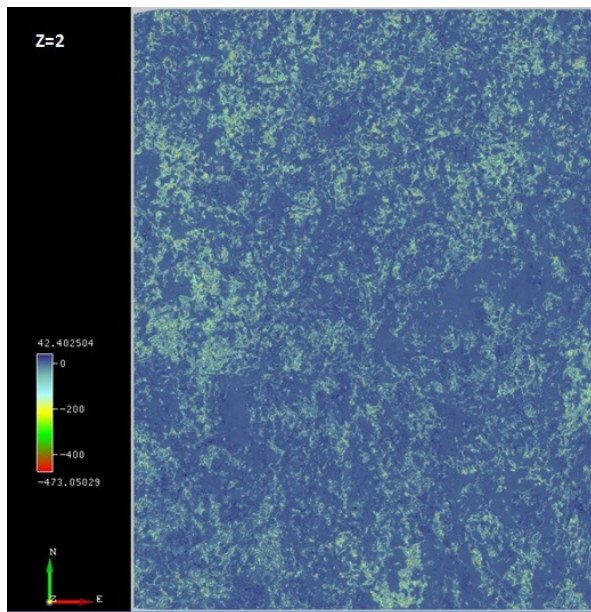
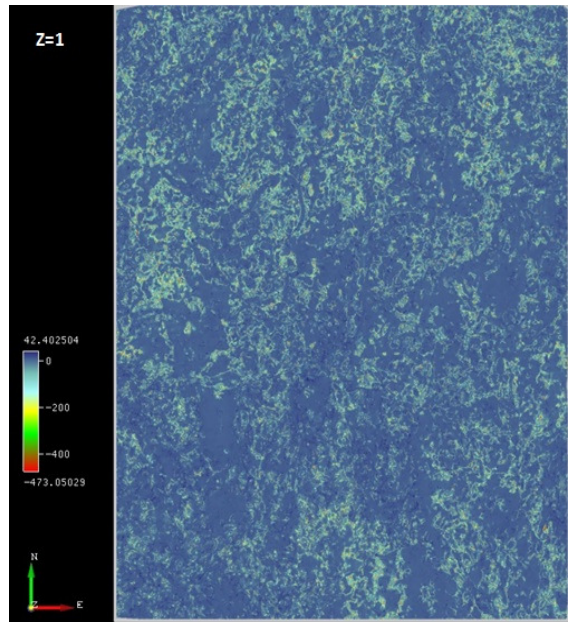
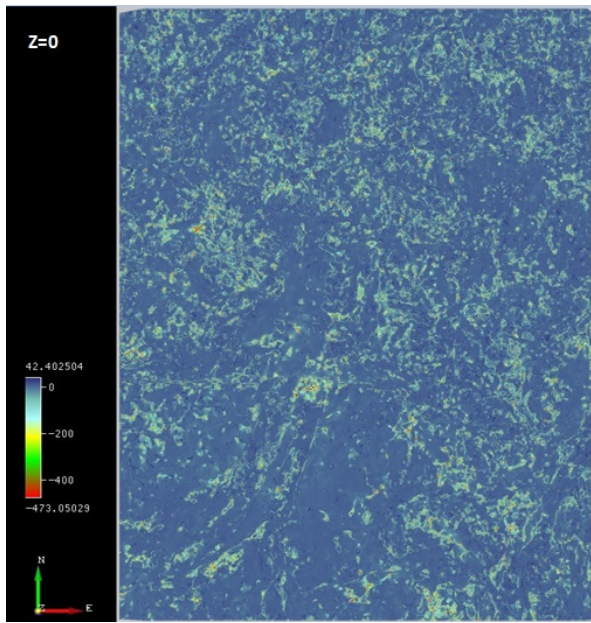
*Cosine of instantaneous phase*



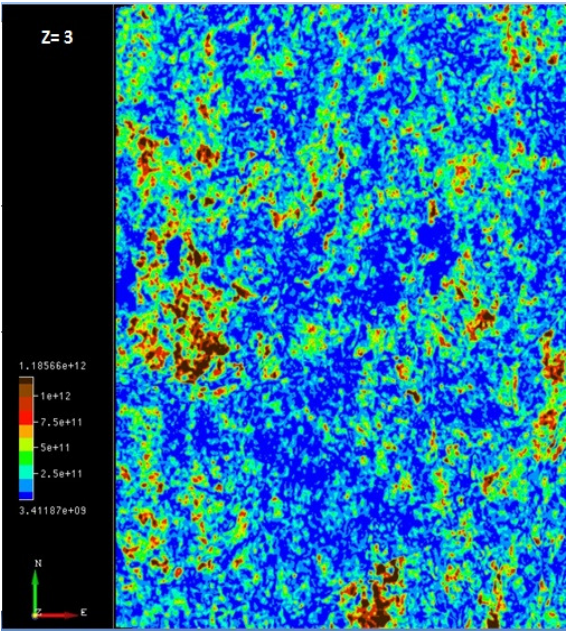
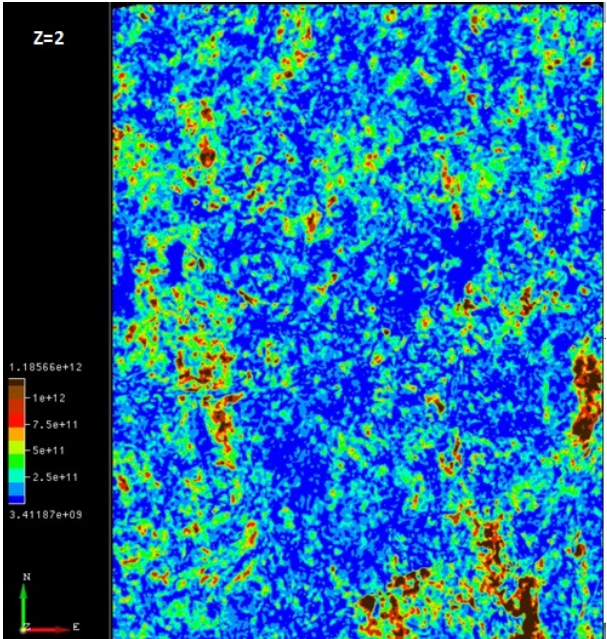
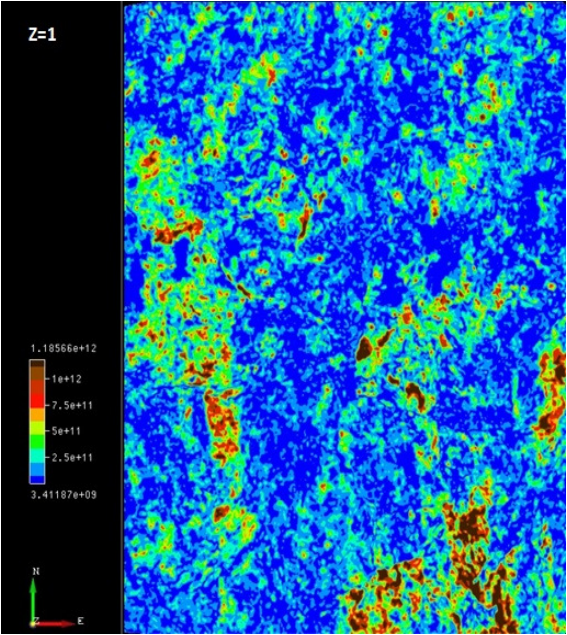
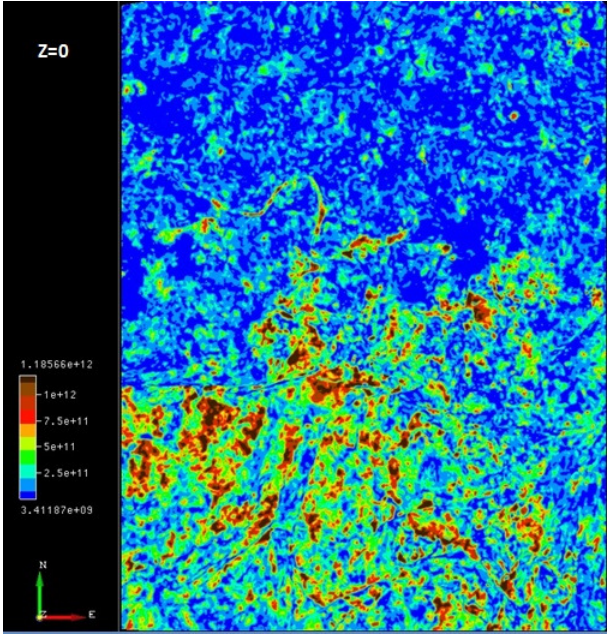
*Thin bed indicator*



*Instantaneous Q factor*

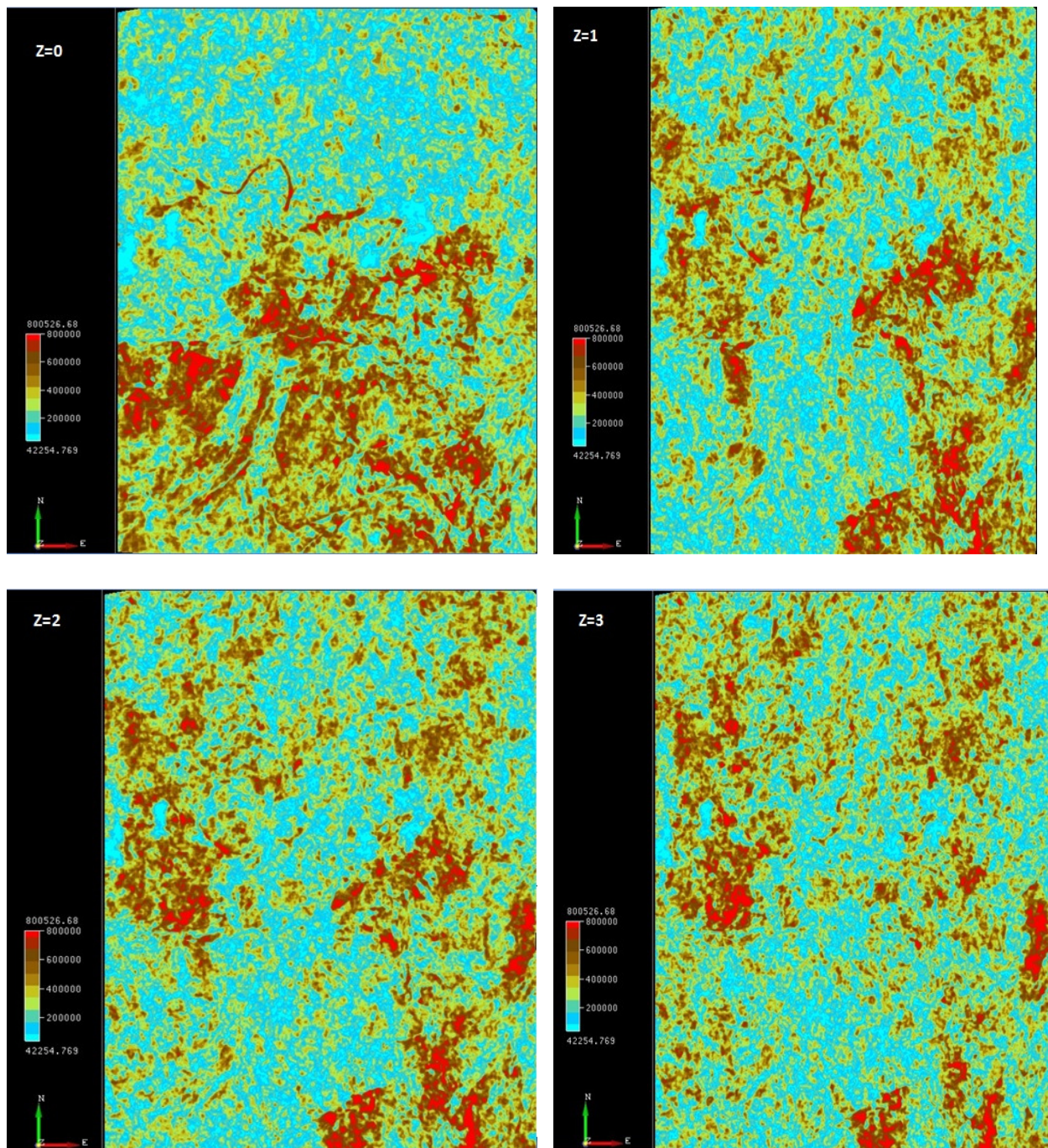


Variance



## *Spectral Decomposition*

The spectral decomposition of at all the three frequencies looked similar.



*RGB display three frequencies*

